Freezing and Capillarity

Axel Huerre, Christophe Josserand, Thomas Séon

Annual Review of Fluid Mechanics

Freezing and Capillarity

Axel Huerre,[1] Christophe Josserand,[2] and Thomas Séon[3,4]

[1]Laboratoire Matière et Systèmes Complexes, Université Paris Cité, CNRS (UMR 7057), Paris, France; email: axel.huerre@cnrs.fr

[2]Laboratoire d'Hydrodynamique, Institut Polytechnique de Paris, CNRS-Ecole Polytechnique (UMR 7646), Palaiseau, France

[3]Institut Franco-Argentin de Dynamique des Fluides pour l'Environnement, CNRS (IRL 2027), Universidad de Buenos Aires, CONICET, Buenos Aires, Argentina

[4]Institut Jean Le Rond d'Alembert, Sorbonne Université, CNRS (UMR 7190), Paris, France

Annu. Rev. Fluid Mech. 2025. 57:257–84

First published as a Review in Advance on September 25, 2024

The *Annual Review of Fluid Mechanics* is online at fluid.annualreviews.org

https://doi.org/10.1146/annurev-fluid-121021-111652

Keywords

solidification, capillarity, ice, wetting, drops

Abstract

Ice structures such as accretion on airplanes, wires, or roadways; ice falls; ice stalactites; frozen rivers; and aufeis are formed by the freezing of capillary flows (drops, rivulets, and films). To understand these phenomena, a detailed exploration of the complex coupling between capillary flow and solidification is necessary. Among the many scientific questions that remain open in order to understand these problems are the confinement of the thermal boundary layer by the free surface, the interaction between a freezing front and a free surface, the effect of freezing on the contact line motion, etc. This review focuses mainly on water and ice, discussing the theoretical framework and recent developments in the main areas of the freezing–capillarity interaction. The text deeply explores the freezing of a moving drop and the fundamental problem of wetting water on ice. Additionally, it highlights some of the main open questions on the subject.

1. INTRODUCTION

1.1. Context

From the splats obtained during surface coating by liquid metal drops (Aziz & Chandra 2000) to 3D printing (Lewandowski & Seifi 2016), from the formation of icicles (Neufeld et al. 2010) to the thawing of the permafrost (McGuire et al. 2018), from the development of mushy layers (Worster 2000, Anderson & Guba 2020) to the dynamics of the sea-ice layer (Feltham et al. 2006), and from a rivulet freezing (Monier et al. 2020) to the dangerous ice accretion on aeronautic structures (Gent et al. 2000, Moore et al. 2017), a wide variety of processes are examples of the subtle interplay that capillarity and melting or solidification can exhibit. **Figure 1** illustrates some of these phenomena for water–ice situations.

These problems involve the coupling between at least three phases, the solid one, its liquid counterpart, and a gas phase. In the following, we use ice for the solid and water for the liquid, although our review applies to general liquid–solid phase change. The three phases are usually in contact with another solid, a substrate, or a container that may play a crucial role in the thermal exchanges (Roisman & Tropea 2021). The major difficulties in dealing with such systems lie in the different interfaces' dynamics: water–ice, water–gas, and gas–ice. Their dynamics couple the heat equation with the conditions at the interface (in particular, the Stefan condition for the phase changes, seen in Equation 4) on one side and the fluid dynamics for the gas and liquid phases, with the corresponding kinematic and dynamic boundary conditions, on the other side. Fundamental issues arise from these coupled dynamics. First, the ice–water system can be understood as a diffusive-boundary value-driven problem, imposing a temperature condition at the interface. Meanwhile, the heat equation in both phases leads to a heat flux, the balance of which is ensured by either the ice melting or the water freezing. In addition, capillary effects at the interfaces can influence these dynamics (e.g., the Gibbs–Thomson effect; see Section 1.3) and, in particular,

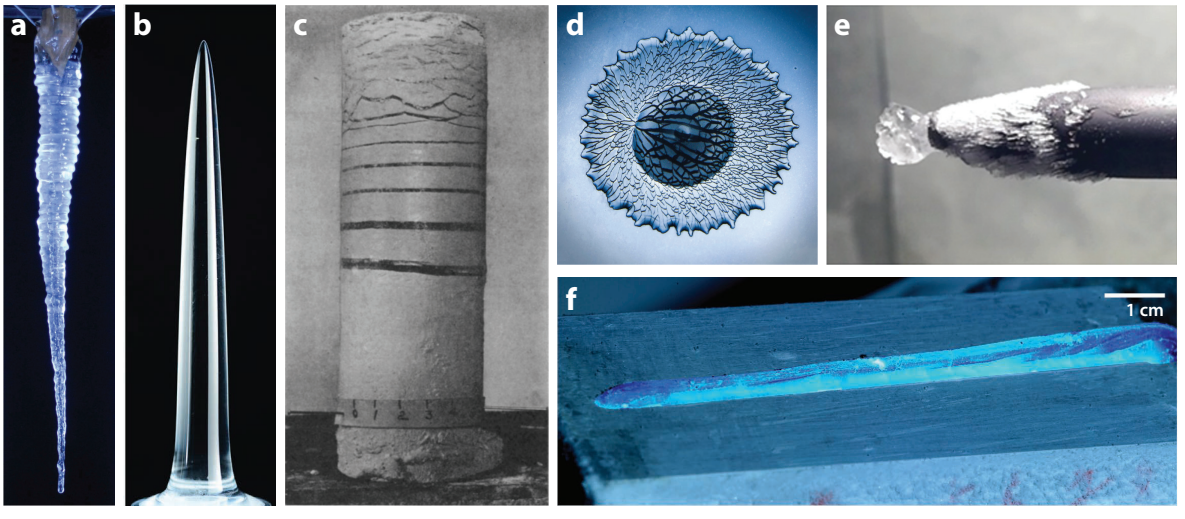

Figure 1

Illustrations of situations where water and ice interact close to a free surface: (*a*) icicle, (*b*) pinnacle from melting ice, (*c*) frozen clay cylinder with pure ice layers appearing, (*d*) cracked frozen splat of ice, (*e*) frozen Pitot sensor, and (*f*) ice shape after a rivulet flow on a cold plate. Panel *a* reproduced from University of Toronto Icicle Atlas (CC BY 4.0), panel *b* reproduced with permission from Weady et al. (2022), panel *c* reproduced with permission from Taber (1930), panel *d* photograph provided by V. Thiévenaz, and panel *f* reproduced from Huerre et al. (2021).

interrogate the wetting properties of the liquid phase on its own solid, thus challenging the thermodynamics of such interfaces.

For these reasons, the field covered in this review has been very active, particularly in the last 20 years, blowing a new wind on an old problem (tracing back to the early nineteenth century) at the crossroads between fluid mechanics, soft matter, heat transfer, and phase change. The present review focuses therefore on recent results in which freezing and capillarity interfere strongly. An emphasis is placed on water–ice configurations, first because of their numerous relevant applications and contexts, and also because they present peculiar properties, such as the dewetting behavior of water on its own solid (Knight 1966). Thereby, this review is divided into three parts: In the first one the theoretical framework is briefly recalled, the second presents the different works on this interaction between capillary flows and freezing, and the third part is dedicated to the unusual wetting of water on ice.

Heat diffusion coefficient: $D_j = \frac{k_j}{\rho_j c_{p,j}}$ with $j = (\mathrm{s}, \mathrm{i}, \mathrm{w}, \mathrm{g})$ for the substrate, ice, water, and gas phases, and where k_j, ρ_j, and $c_{p,j}$ are the thermal conductivity, the density, and the heat capacity for each phase, respectively

μ: viscosity, with μ_w and μ_g the water and gas dynamical viscosities

1.2. Physical Model

To characterize the scientific challenges of the problem, it is interesting to consider the physical equations to be solved for the general situation where an ice–water system is in contact with a cold solid substrate and surrounded by air (see **Figure 2*a***). In the following, the subscript j for the different variables will denote the different phases: s for the substrate, i for the ice, w for the water, and g for the gas. We choose the ice–water system to describe the model but it could be applied to any solid–liquid couple.

For such a configuration, the momentum and energy equations have to be considered; they are written here in terms of the temperature and velocity fields, T_j and $\mathbf{u}$, respectively:

- In the solid substrate and in the ice, neglecting thermal deformation, we have only the heat diffusion equation ($\mathbf{u} = \mathbf{0}$):

$$\frac{\partial T_j}{\partial t} = D_j \Delta T_j, \qquad 1.$$

where D_j is the heat diffusion coefficient. All the thermal coefficients are considered constant in each phase.

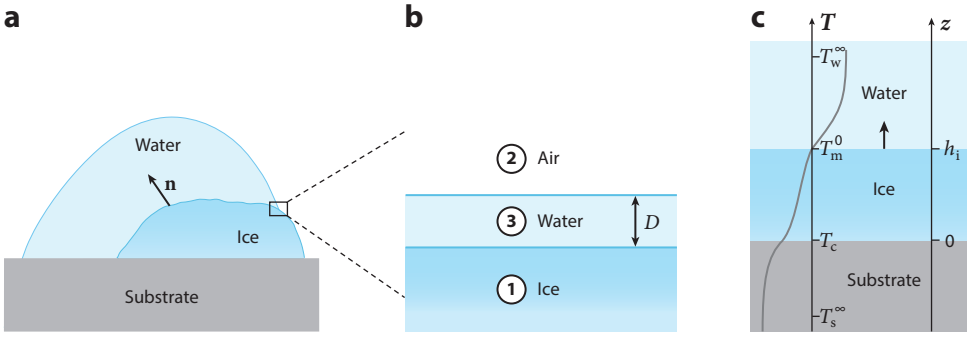

Figure 2

(*a*) General scheme of the problem of water freezing from a cooled substrate. The ice–water interface is defined by its normal **n**. (*b*) Magnified view of the configuration where a thin film of water of thickness D exists on the ice. (*c*) The 1D solidification problem, with the notations used in the model for the temperatures and the vertical positions.

- In the water and the gas, taken as Newtonian fluids, the heat equation is coupled with the velocity that obeys the incompressible Navier–Stokes equation

$$\frac{\partial T_j}{\partial t} + \mathbf{u}_j \cdot \nabla T_j = D_j \Delta T_j, \qquad 2.$$

$$\rho_j \left(\frac{\partial \mathbf{u}_j}{\partial t} + \mathbf{u}_j \cdot \nabla \mathbf{u}_j \right) = -\nabla p_j + \nabla(2\mu_j \mathcal{D}_j) + \rho_j \mathbf{g}, \text{ and } \nabla \cdot \mathbf{u}_j = 0, \qquad 3.$$

where $\mathcal{D}_j = \frac{1}{2}(\nabla \mathbf{u}_j +^t \nabla \mathbf{u}_j)$ is the rate of strain tensor and ρ_j and μ_j are the fluid densities and dynamical viscosities, a priori depending on the temperature.

Latent heat of solidification ($\mathcal{L}_f$): the heat per unit mass that is released (absorbed) when ice forms (melts); for ice–water, $\mathcal{L}_f = 336\,\text{kJ kg}^{-1}$, large compared to most other elements

These coupled heat and momentum equations interact through the boundary conditions at the different interfaces. Since this review focuses on the liquid–solid phase change (melting–solidification), we neglect here the gas–liquid and gas–solid phase changes (evaporation–condensation–sublimation). Therefore, within this approximation, we have the continuity of the temperature field at each interface and that of the thermal flux $-k_j \nabla T$ through the interfaces where phase change is absent or can be neglected. The remaining interface, water–ice, is the one driving the dynamics. There, the temperature is imposed to be the melting one T_m. Consequently, the thermal fluxes across such interface have no reason to match, leading to the well-known Stefan boundary condition:

$$\rho_\text{i} \mathcal{L}_f \mathbf{v}_\text{iw} \cdot \mathbf{n} = (k_\text{i} \nabla T_\text{i} - k_\text{w} \nabla T_\text{w}) \cdot \mathbf{n}, \qquad 4.$$

where $\mathbf{v}_\text{iw}$ is the velocity of the interface due to the ice–water phase change, $\mathbf{n}$ the normal vector to the interface oriented from the solid to the liquid phase, and $\mathcal{L}_\text{f}$ the mass latent heat of solidification. With all these equations and the boundary conditions, the system is now well-posed.

1.3. Gibbs–Thomson Effect, Kinetic Undercooling

As a first approximation T_m can be considered constant ($T_\text{m}^0 = 0°\text{C}$, for water–ice), but it depends on both the geometry of the interface and its velocity primarily. First, the thermodynamical equilibrium at the interface leads to the Gibbs–Thomson effect, relating the melting temperature to the local interface curvature through the water–ice surface tension. Then the kinetic of phase change imposes a dependence of the melting temperature on the interface velocity, making it harder to solidify when the velocity increases (Worster 2000). Therefore, the melting temperature $T_\text{m}(\mathbf{x}, t)$ depends on space and time, yielding

$$T_\text{m}(\mathbf{x}, t) = T_\text{m}^0 - \epsilon_\kappa \kappa - \epsilon_v \mathbf{v}_\text{iw} \cdot \mathbf{n}, \qquad 5.$$

where ϵ_κ and ϵ_v are the surface tension and kinetic coefficient, κ being the local curvature of the interface (defined according to the normal vector $\mathbf{n}$).

1.4. Ice Front Dynamics

Heat is released (absorbed) when ice forms (melts), and it is crucial to determine where this heat is coming or extracted from. In general, both the water and ice phases contribute to the global heat flux balance, but two idealized configurations are important to consider since they are key ingredients to understanding solidification–melting dynamics.

1.4.1. Planar growth: the Stefan problem. First introduced by Lamé and Clapeyron (see the sidebar titled Lamé–Clapeyron Historical Derivation), the Stefan problem is generally associated with Josef Stefan, who derived it in the late nineteenth century. It is still largely used and pertinent to characterize the properties of planar ice growth (Loulou & Delaunay 1997, Thiévenaz et al. 2019, Worster 2000). We present here its generalized configuration in one dimension in which

LAMÉ–CLAPEYRON HISTORICAL DERIVATION

The exploration of heat's fundamental role in shaping our world began with Joseph Fourier's groundbreaking work in 1807, leading to the development of his influential heat equation in 1822. Less than a decade later, Gabriel Lamé and Émile Clapeyron embarked on a pioneering investigation into the dynamics of solidification (Lamé & Clapeyron 1831). Inspired by Fourier's insights, they sought to unravel the mysteries surrounding the Earth's formation and age. Their research proposed the idea that the Earth's crust formed through the gradual cooling and solidification of its original molten state. Utilizing a simplified 1D model and the newly formulated heat equation for solids, they delved into the complex process of heat transfer during solidification. Despite their efforts, they encountered challenges in fully resolving the problem, lacking tools to solve the integral formulation they obtained. Though their quest did not yield a definitive solution, their pioneering work laid the foundation for further inquiry into fundamental processes governing solidification dynamics.

the ice grows from a cold substrate (see **Figure 2*c***). The water temperature far from the ice is supposed constant (T_w^∞) as well as the substrate temperature ($T_s^\infty < T_m$); the kinetic undercooling is neglected here ($T_m = T_m^0$). The flow is neglected in this purely diffusive problem so that the diffusion equation (Equation 1) holds for each temperature field $T_{j=s,i,w}(z, t)$. At the ice–water interface $z = h_i(t)$, we have the melting temperature T_m^0 and the Stefan condition reads

$$\rho_i \mathcal{L}_f \frac{dh_i}{dt} = k_i \frac{\partial T_i}{\partial z} - k_w \frac{\partial T_w}{\partial z}. \quad 6.$$

Together with the continuity of the temperature and the heat fluxes at $z = 0$, this allows for a self-similar solution for the temperature fields involving the self-similar variable $z/\sqrt{t}$, yielding for the ice front (Roisman 2010b, Thiévenaz et al. 2019)

$$h_i(t) = \lambda\sqrt{D_i t} = \sqrt{D_{\text{eff}} t}, \quad 7.$$

where λ is the solution of the transcendental equation

$$\frac{e^{-\left(\frac{\lambda}{2}\right)^2}}{\text{Erf}\left(\frac{\lambda}{2}\right) + \frac{e_i}{e_s}} + \bar{T}\frac{e_w}{e_i}\frac{e^{-\left(\frac{\lambda}{2\alpha_l}\right)^2}}{1 - \text{Erf}\left(\frac{\lambda}{2\alpha_l}\right)} = \frac{\lambda\sqrt{\pi}}{2St}, \quad 8.$$

with $\text{Erf}(x) = \frac{2}{\sqrt{\pi}}\int_0^x e^{-\xi^2} d\xi$, $\alpha_l = \sqrt{D_w/D_i}$ the ratio of diffusivities between the water and the ice, and the reduced temperature $\bar{T} = (T_w^\infty - T_m^0)/(T_m^0 - T_s^\infty)$. We have also introduced the effusivity of the materials and the Stefan number.

It is important to notice that in this self-similar framework, the contact temperature at the interface between the substrate and the ice is a constant:

$$T_c = T_s^\infty + \frac{T_m^0 - T_s^\infty}{1 + \frac{e_s}{e_i}\text{Erf}\left(\sqrt{\frac{D_{\text{eff}}}{4D_i}}\right)}. \quad 9.$$

Asymptotic regimes can be deduced from Equation 8 in the case $\bar{T} = 0$: $D_{\text{eff}} \sim D_i St^2$ and $T_c = T_m^0$ for $St \ll 1$; $D_{\text{eff}} \sim D_i \ln(St)$ and $T_c = (e_s T_s^\infty + e_i T_m^0)/(e_s + e_i)$ for $St \gg 1$. Note that for highly effusive substrates ($e_s \gg e_i$), we find that $D_{\text{eff}} \sim D_i St$ and $T_c = T_s^\infty$ for $(e_i/e_s)^2 \ll St \ll 1$, recovering the case where the substrate effect is reduced to an imposed temperature at $z = 0$. Finally, the stability analysis of this solution (Langer 1980) leads to the classical Mullins–Sekerka instability (Mullins & Sekerka 1964) when the water is supercooled ($T_w < T_m^0$), at the origin of the dendritic growth of the ice.

Undercooling: the undercooling ΔT is the temperature difference between the substrate temperature and the melting one, $\Delta T = T_m^0 - T_s^\infty$

Effusivity (e_j): a material's effusivity, $e_j = \sqrt{\rho_j c_{p,j} k_j}$ characterizes its ability to exchange heat

Stefan number (St): compares the sensible heat of a material with the energy for solidification: $St = \frac{c_{p,i}(T_m^0 - T_s^\infty)}{\mathcal{L}_f}$

Contact temperature (T_c): the effective temperature at the ice–substrate interface during the solidification process

Supercooling: a supercooled liquid is in a metastable state with the liquid at a temperature below its melting temperature (for water, $T_w < 0$°C)

1.4.2. Dendritic growth. When the water is supercooled, the growth of the ice is not planar anymore but is dominated by dendrites: The latent heat is absorbed in the water and its diffusion from the interface drives the dynamics. When considering an infinite domain of supercooled water, the dendrite solution appears as a paraboloid whose constant growing speed and fixed tip curvature are selected by the Gibbs–Thomson effect through the matching of the temperature field between the tip region and the far field region (Langer 1980). While such asymptotic methods can predict the relation between the dendrite velocity V_d and the water temperature T_w for small undercooling, only an empirical law has been obtained experimentally for larger undercooling (Shibkov et al. 2005):

$$V_d = K(T_m^0 - T_w)^\gamma, \qquad 10.$$

with $K = 4.83 \times 10^{-5}$ SI and $\gamma = 2.78$.

1.4.3. Crystal nucleation and recalescence. With the two asymptotic ice growth regimes described above, planar and dendritic, we can now infer more complex ice formation regimes. For instance, when a drop is placed in contact with a cold substrate (Stiti et al. 2020), the planar ice front does not appear immediately because ice seeds need first to be nucleated at the substrate interface (Schremb et al. 2017). In general, nucleation of these crystals appears when the liquid water is supercooled by the substrate, and nucleation theory can be applied to determine the probability and the distribution of the crystals (Fanfoni & Tomellini 1998, Koldeweij et al. 2021). This is followed by a rapid expansion of the dendrites inside the drop, called the recalescence stage. Then the water is at the melting temperature all over the droplet, and a quasi-planar front ice growth regime is observed (Jung et al. 2012a). When the water is supercooled $T_w < T_m^0$, the Stefan number based on this temperature difference $St = \frac{c_{p,w}(T_m^0 - T_w)}{\mathcal{L}_f}$ gives the proportion of water that can solidify during the recalescence regime.

1.5. Numerical Methods

Solving the set of Equations 1–3 is particularly challenging because of the boundary conditions of Equations 4 and 5 and because of the sharp interface framework. Accurate numerical methods need to deal with both sharp interfaces, similar to a usual liquid–gas system (Tryggvason et al. 2011), and the specific boundary value problem at the interface, involving a precise estimate of the temperature gradients. Although the subject traces back to the early 1980s, we focus in this paragraph on recent numerical developments. As for multifluid numerical modeling, two main families of methods can be used, front-tracking ones where the position of the interface is explicitly stored and front-capturing ones where the interface position is determined implicitly (Jaafar et al. 2017). Front-tracking methods have been developed, in particular, for dendritic growth analysis (Juric & Tryggvason 1996, Reuther & Rettenmayr 2014), exhibiting good accuracy on the one hand but difficulties in handling coalescence of ice domains on the other hand. The other type of methods involve an implicit account of the interface, and different approaches have been developed. Among them are those describing a thick interface at the solidification front; in particular, the enthalpy method uses a continuous formulation of the energy equation taking into account the phase change (Ulvrová et al. 2012, Lyu et al. 2021), while the phase-field method takes advantage of an external continuous field to characterize the front (Boettinger et al. 2002, Plapp 2011, Favier et al. 2019). Other approaches use a sharp interface description of the front thanks to level-set methods often coupled with specific models for the solid phase (Gibou et al. 2018, Limare et al. 2023). However, most of these numerical methods concern a water–ice system, and a main challenge for future development consists of incorporating both a solid substrate and the surrounding air into the model, which should involve hybrid approaches (Tavares et al. 2024).

THE BYZANTINE FROZEN DROP

Stairs (1971) first noticed something intriguing about frozen water droplets, which he aptly named the Byzantine shape. In an experiment, he deposited water on an aluminum rod immersed in a freezing mixture, resulting in a frozen droplet with a spherical base. However, as the solidification front rose, the top showed a sharp cusp with an inflection point. He explained this phenomenon qualitatively using two key geometrical factors: (*a*) The volume of ice was greater than that of water and (*b*) the liquid formed a part of a sphere.

As can be noticed in the typical picture obtained after a water droplet freezes (**Figure 3*a***), the curvature of the interface changes its sign near the tip. Unfortunately, a model considering only the two previous ingredients failed to recover this feature. Despite these insights and later captivating images by Walford et al. (1991), the mystery lingered about the physical factors behind this curvature change.

Twenty-five years later, Anderson et al. (1996) brought attention to the trijunction condition (ice–water–air) in shaping the frozen interface. The local thermal equilibrium at this point (Schultz et al. 2001) revealed that the solidification front must locally be orthogonal to the vapor–water interface, challenging the flat-front assumption made in early models. This crucial observation was later experimentally confirmed (Nauenberg 2013, Stiti et al. 2020, Séguy et al. 2023). Notable attempts to theoretically find the tip angle assumed the ice–water front as a part of a sphere and the solidified cusp as a cone (Schetnikov et al. 2015, Nauenberg 2016). These geometric constraints, along with the volume increase due to ice formation, resulted in a universal angle of 130°, confirmed by experiments for different sizes and substrate temperatures (Marín et al. 2014). These models are well suited to describe the simple problem for water, but recent experiments, calling for more refinements, challenged them by introducing pollutants to the water (Boulogne & Salonen 2020) or modifying heat flux balances at the trijunction (Sebilleau et al. 2021, Miao et al. 2024), leading to different angles and even different geometries.

2. FREEZING CAPILLARY OBJECTS

When solidification of a liquid capillary object occurs, several mechanisms come into play, potentially altering its characteristics. First, the phase change is accompanied by a volume variation, which in turn modifies the object's geometry and so the interface's shape, an important parameter when looking at capillary objects. Second, the formation of new solid phases creates additional interfaces, generating, in particular, new contact lines (with their dissipation singularities) and potentially even giving rise to quadruple points (Herbaut et al. 2020). The wetting properties, dependent on the phases' interaction, can also vary, which raises the question of the particular situation of a liquid wetting its own solid phase. Third, phase change involves latent heat, necessitating its transfer through the surrounding media. The liquid–air interface may act as a no-flux boundary condition for heat transfer, and the thermal boundary layer might be confined by the interface (Gielen et al. 2020, Huerre et al. 2021). Finally, the quintessential object for studying capillarity is the droplet. When a drop of water is deposited on a cold substrate, it undergoes freezing, gradually forming a distinct Byzantine shape (see the sidebar titled The Byzantine Frozen Drop), involving two of the aforementioned mechanisms: volume change and the thermal boundary condition at the triple point. Furthermore, drop impact dynamics can be directly modified by the freezing, such that the splashing transition on cold substrates behaves as for the impacts on hydrophobic surfaces (Grivet et al. 2023). In this section, we thus focus on the coupling between freezing and drop dynamics.

2.1. Freezing a Moving Drop

Thinking about a drop solidifying while moving, one can describe several scenarios depending on the source of the cooling. If it comes from the ambient air, evaporative cooling and/or cold

temperatures could lead to droplet solidification, most of the time inducing supercooling. Despite its importance for the physics of clouds (Khain & Pinsky 2018) and the interplay between droplets and frost (Jung et al. 2012a,b), this case is not treated in this review. On the other hand, if the heat flux comes from a cold surface, all of the effects mentioned in Section 1 could take place and we have the classic situation involving capillary phenomena and solidification.

Deposition: when a drop is gently put in contact with a substrate; the driving force for spreading is capillarity

Impact: the drop impacts the substrate with a prescribed velocity U; the driving force for spreading is the drop's inertia

Reynolds number (*Re*): compares inertial and viscous forces: $Re = \frac{UR_0}{\nu}$, with ν the kinematic viscosity and U the impact velocity

Weber number (*We*): compares inertial to surface tension forces, $We = \frac{\rho U^2 R_0}{\gamma}$

Impact parameter (*P*): defined as $P = We\,Re^{-2/5}$ and links the capillary-dominated regime ($P \ll 1$) to the viscous-dominated one ($P \gg 1$)

2.1.1. Spreading characteristics in isothermal conditions. When a drop of volume $\propto R_0^3$ encounters a solid surface, it spreads during a time τ_s. After this time, the contact line can either stay in this position (deposition) or recede (impact). With an impact, a lot of other phenomena can be also triggered (prompt splash, corona splash, receding breakup, partial rebound, or complete rebound). The radius at $t = \tau_s$ is maximal, R_{max}, and there is a huge amount of literature looking at the relationship between the spreading factor $\beta_{max} = R_{max}/R_0$ and impact characteristics (Yarin 2006, Josserand & Thoroddsen 2016). We quickly go through the basics of spreading for the case of a droplet deposited on a surface and for a droplet impacting the surface with a characteristic velocity U.

2.1.1.1. Spreading after droplet deposition. After touching the substrate, the droplet falls and a curvature gradient is created near the contact line. This strong curvature generates a capillary pressure gradient that is resisted by the inertia of the liquid. It leads to the relation $r(t) \propto \sqrt{t/\tau_c}$ (Biance et al. 2004), where $\tau_c = \sqrt{\rho R_0^3/\gamma}$ is the inertia–capillary time.

After a long time (typically a few τ_c), the spreading is limited by the viscosity and the drop relaxes toward its equilibrium shape with a contact angle θ_e. This gives the relation for the spreading ratio

$$\beta_{max}^D = \left(\frac{4 \sin^3 \theta_e}{2 + \cos^3 \theta_e - 3 \cos \theta_e} \right)^{1/3}. \qquad 11.$$

2.1.1.2. Spreading after an impact. For a droplet impacting the substrate with a velocity U, the spreading factor can take different forms (Josserand & Thoroddsen 2016). The dynamics is more complex, but the experimental data are well described by the general equation (Laan et al. 2014)

$$\beta_{max}^I \sim Re^{1/5} \frac{P^{1/2}}{A + P^{1/2}}, \qquad 12.$$

with $A = 1.24$ and $P = We\,Re^{-2/5}$ the impact parameter. This expression recovers the classical scaling $\beta_{max}^I \sim We^{1/2}$ for $P \ll 1$ and $\beta_{max}^I \sim Re^{1/5}$ for $P \gg 1$.

2.1.2. Spreading characteristics on a cold surface. We now focus on the cases where this spreading phase is coupled to solidification so that the droplet can be arrested before reaching R_{max}. Both the droplet radius $r(t)$ and the height $h(t)$ are linked through the conservation of mass: $h(t) \times r(t)^2 \propto R_0^3$ and the substrate is at a temperature $T_s < T_m$ (see **Figure 3*b***).

2.1.2.1. Spreading dynamics on cold surface. Many experiments have recently shown that the dynamics of a spreading drop is not influenced by the undercooling for any type of impact (gentle or not). For deposition, experiments with water and hexadecane on different substrates (de Ruiter et al. 2017, Grivet et al. 2022, Lolla et al. 2022) recover $r(t) \propto \sqrt{t/\tau_c}$ at short times for all the temperatures tested. Interestingly it seems that the change of the constitutive parameters of the liquids (viscosity, density, surface tension) are not important enough to modify this scaling law (see **Figure 4*d*,*e***) with no effects of the temperature at early times). For impacts on cold surfaces, similarly, experiments were run with eutectic solder (Attinger et al. 2000), water (Grivet et al. 2023), wax (Bhola & Chandra 1999), and tin (Gielen et al. 2020), showing a negligible effect of the temperature on the initial dynamics of spreading.

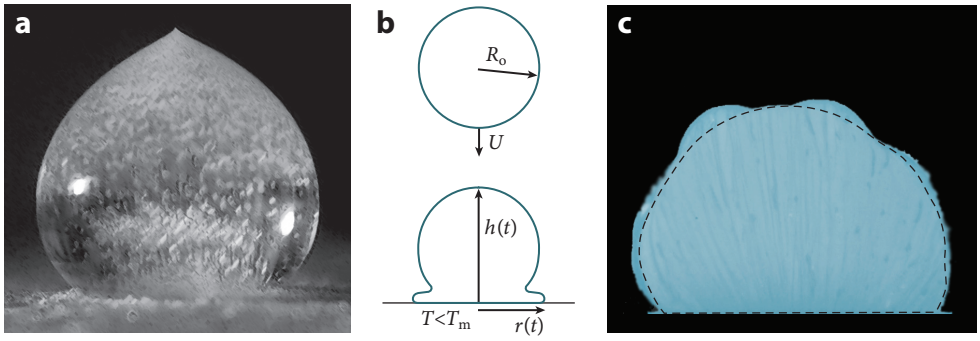

Figure 3

(*a*) Frozen sessile droplet. Panel adapted with permission from Schetnikov et al. (2015). (*b*) Schematics of a drop impact and consequent spreading. (*c*) Complex shape obtained after a drop of hydrogel is frozen (*dashed line* is for the initial shape). Drops in both panel *a* and panel *c* have a diameter of 3 mm. Photograph provided by L. Séguy.

2.1.2.2. Droplet spreading arrest after deposition. As shown in **Figure 4*d***, the unaltered spreading dynamics is suddenly stopped and the arrest radius is constantly found to decrease with undercooling. Different mechanisms have been explored to explain this relation between spreading and solidification, involving bulk freezing mechanisms (Lolla et al. 2022), contact line

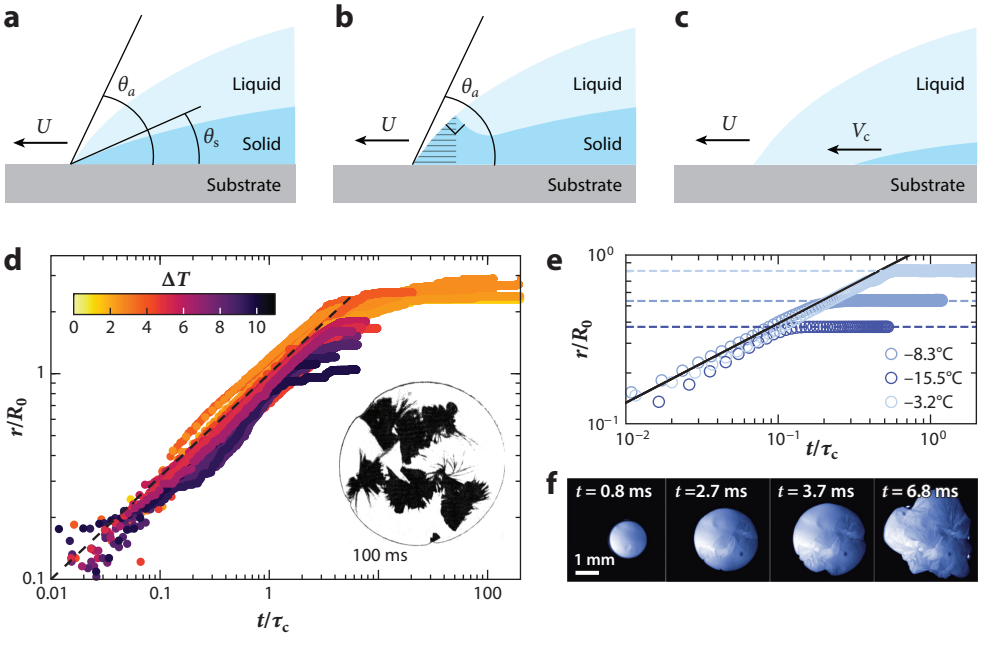

Figure 4

Arrest of spreading of a drop due to solidification. (*a*) The contact line is stopped when the two angles are equal. (*b*) The drop stops spreading when a critical volume of solid is formed at the contact line. (*c*) The contact line is arrested when the crystal is able to catch it: $V_c > U$. (*d*) The spreading factor as a function of the scaled time for different substrate temperatures ($\Delta T = T_m - T_s$) for hexadecane with an image of the contact line pinning (*inset*). Panel adapted with permission from Koldeweij et al. (2021). (*e*) Radius evolution for water. (*f*) Corresponding time-sequence images with crystal growth and pinning at 3.7 ms, $\tau_c \sim 20$ ms. Panels *e* and *f* adapted with permission from Grivet et al. (2022).

conditions, and the interaction between the solid and the free surface. We describe below the main scenarios identified so far.

When a contact line condition is invoked for the arrest, a localized effect due to solidification at the contact line stops the drop (**Figure 4*a*,*b***). Whether the blockage occurs when the slope of the free surface (decreasing when spreading) is equal to the slope of the edge of the solid (Schiaffino & Sonin 1997a,b), when the volume of ice created at the contact line reaches a critical value (Tavakoli et al. 2014), or when both effects appear (Herbaut et al. 2020), a reasonable agreement between these models and experimental data was obtained. Note that all the experiments were performed with hexadecane or molten wax and that the spreading is forced through continuous feeding of the liquid and for a reduced range of temperatures. It should be emphasized, however, that those theories imply a strong modification of the liquid flow near the contact line, which in the case of self-spreading of droplets would lead to a strong dependence of the radius dynamics with the thermal parameter.

When there is interaction between the solid and the free surface, the contact line is caught by a crystal growing near the substrate (**Figure 4*c***). This hypothesis was tested successfully for different substrates, liquids, and temperature ranges with good agreement between the models and the experimental measures. Very recent experiments by Koldeweij et al. (2021) on hexadecane droplets directly visualized the growth of the solid layer, measured the crystal velocity V_c, and identified the interaction of the crystal with the contact line as the trigger for the drop arrest (**Figure 4*d***, inset). The spreading factor diminution with the undercooling, ΔT, confirms previous results on different substrates (de Ruiter et al. 2017). Interestingly, de Ruiter et al. (2017) noticed that more conductive substrates lead to smaller spreading factors. Pushing forward this dependency, Grivet et al. (2022) performed a series of experiments with water deposited on sapphire and in situ measurements of the ice growth velocity (**Figure 4*f***). They showed good agreement with a model of crystal growth near a conductive substrate and confirmed the observations made with hexadecane: When the crystal is able to reach the contact line ($V_c > U$), the drop stops. This criterion was also proposed for the forced motion of a contact line of hexadecane on a silicon wafer (Herbaut et al. 2019). The main experimental results from this set of deposition studies are summarized in **Table 1** and illustrate the need for an extended set of experimental data.

2.1.2.3. Droplet spreading arrest after impact. The impact of molten droplets on cold substrates was increasingly studied with the development of metallic spray coating in the 1990s and additive manufacturing afterward. Pioneering work by Madejski (1976) examined both experimentally and theoretically the impact of molten alumina drops at high velocity. The author

Table 1 Experimental dependence of the arrest radius with the undercooling

Reference	Liquid	Substrate	ΔT range	β_{max}	V_c
Tavakoli et al. 2014	Alkanes (C_5, C_6, C_{12})	Glass	1–10	$\Delta T^{-1/3}$	NA
de Ruiter et al. 2017	Alkane (C_6)	Copper, glass	2–12	ΔT^{-1}	ΔT
Herbaut et al. 2019	Alkanes (C_5, C_6)	Silicon wafer	0.2–5	NA	$\Delta T^{2.65}$
Koldeweij et al. 2021[a]	Alkane (C_6)	Saphire	2–4	ΔT^{-1}	ΔT
Grivet et al. 2022[a, b]	Water	Saphire	3–25	ΔT^{-1}	ΔT
Lolla et al. 2022	Water	Ice	10–30	$\frac{T_l - T_f}{T_l - T_s}^{1/7}$	NA

$\beta_{max} = R_{max}/R_0$ and V_c is the crystal growth velocity.
[a]The substrate is considered at the contact temperature T_c.
[b]A refinement of the model captures the data at high ΔT but breaks the simple scaling law.
Abbreviation: NA, not available.

performed an energy balance between the falling molten drop and the subsequent splat to derive a prediction for β_{max}. The solidifying layer appears in the calculation of both the kinetic energy (a part of the liquid mass is lost to solidification) and in the work of the viscous forces (the height of the liquid layer is modified). With this approach, the author recovers both the $We^{1/2}$ and $Re^{1/5}$ asymptotic regimes of β_{max} for the isothermal case. The solidifying case is studied numerically but when both *We* and *Re* are high, we can rewrite the asymptotic regime the author finds as $\beta_{max} \sim (Re\,Pr)^{1/5} St^{-2/5}$. When the undercooling is increased, *St* increases and the final radius of the splat is reduced. Following this path and considering only the effect of solidification in the kinetic energy term, Pasandideh-Fard et al. (1998) highlighted the importance of the thermal contact resistance. Indeed, liquid metals have an effusivity similar to the cold substrate and thus the thermal boundary conditions imposed have to be carefully thought out; they cannot be approximated by a substrate constant temperature. This point was further highlighted in a book chapter by Poulikakos et al. later on (Poulikakos et al. 2002). A similar behavior was measured for solder impacts ($P \ll 1$): The spreading is arrested earlier for lower substrate temperatures (Attinger et al. 2000), which is attributed to potential solidification at the contact line.

Prandtl number (*Pr*): compares the viscous and thermal boundary layer thicknesses, $Pr = \frac{\nu}{D}$, with *D* being the thermal diffusivity

To rationalize those findings, Roisman (2010a) performed a theoretical analysis of axisymmetric flows (following a drop impact, for example) with a phase change at the boundary. Solving the Navier–Stokes equation coupled to advection–diffusion for the temperature, the author highlighted the strong coupling between the flow and the temperature fields. In particular for molten tin impacting on stainless steel, for undercoolings greater than 50°C, the solution of the solid layer growth differs significantly from the Stefan solution (see Section 1.4.1), in agreement with the experiments. The author did not explore the arrest criteria for an impacting droplet but gave a full model for $r(t)$ and $h_i(t)$ that could prove useful in predicting an arrest radius. A perspective on this topic was recently published by Roisman & Tropea (2021). Roisman's model hypothesizes that the solid starts to grow as soon as the liquid touches the substrate. However, for the impact of wax droplets on aluminum, the time to spread is much smaller than the characteristic time to solidify, and consequently the dependence observed with the substrate temperature was attributed to the change of the physical parameters of the impact (Bhola & Chandra 1999, Li et al. 2008).

We notice here that the interplay between the solidification and spreading timescales is critical. To explore this, Kant et al. (2020) performed experimental visualizations of the crystal growth at the substrate surface during the impact of hexadecane drops on cold sapphire. With a small undercooling, they noticed that the drop reaches its maximum viscous damped spreading radius (Equation 12, $P \gg 1$) before a crystal nucleates at the contact line and prevents the drop from recoiling. This delay could explain other experiments with water droplets impacting very smooth silicon wafers where an effect of the undercooling is observed only for $\Delta T > 20$°C (Chang et al. 2021). For higher undercooling, nucleation is observed everywhere during the spreading, except at the contact line. The drop stops before a crystal can be seen reaching the contact line, pointing toward a different mechanism described hereafter for the arrest. These experiments confirmed previous observations of the crystal growth for molten tin on glass (de Ruiter et al. 2018) and for tin on sapphire (Gielen et al. 2020), where the solid layer was always observed very distinctly away from the contact line.

In the quest to find a mechanism that stops a droplet from spreading during impact with solidification, a series of recent papers converged toward a scenario that fits well with several experimental data. The idea is to use the classic argument of the viscous-damped arrest: The drop stops when the liquid layer that spreads reaches a height $h(t)$ comparable to the thickness of the viscous boundary layer. However, this viscous boundary layer develops not from the substrate, as for the isothermal case, but from a growing layer of solid.

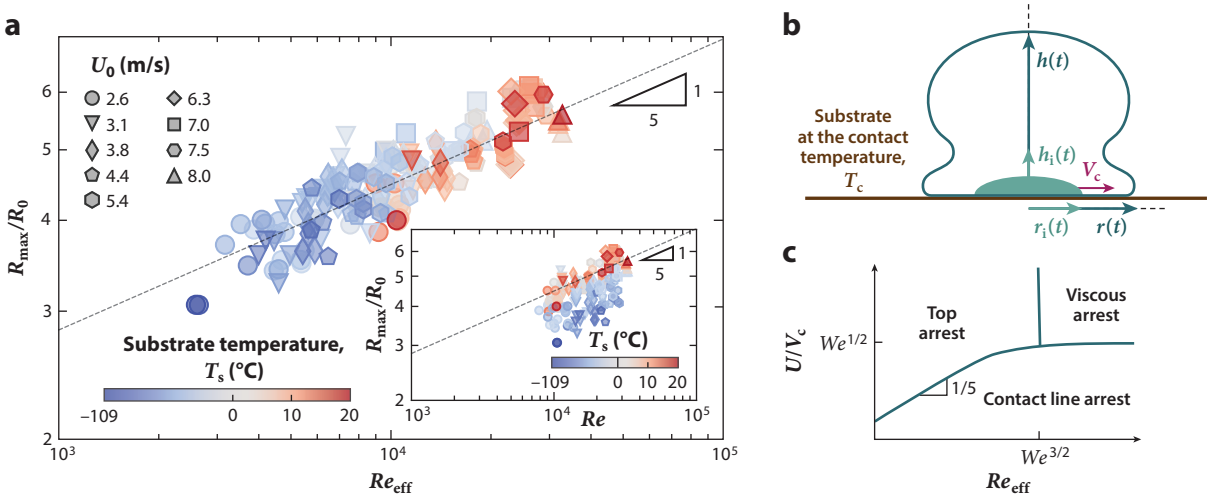

Figure 5

(*a*) Spreading factor as a function of the rescaled Reynolds number (Equation 13). The inset shows original data plotted against the Reynolds number. Panel adapted with permission from Thiévenaz et al. (2020b). (*b*) Schematics of the impacting droplet with the solid growing in the horizontal and vertical directions. (*c*) Possible diagram of the arrest mechanism for a drop impact.

For liquid metals with a very small Pr, the viscous boundary layer is very small compared to the thermal one, and thus the arrest mechanism could be reduced to the meeting of the solid layer with the free surface. This approach was developed by Gielen et al. (2020), using $h(t) \sim R_0(R_0/Ut)^2$ and $h_i(t) \sim \sqrt{D_i\, St\, t}$. Equating those two equations gives a scaling for the arrest, $\beta_{max} \sim (Pr/St)^{1/5} Re^{1/5}$, that works fairly well with their experiments with molten tin.

For water, however, one has to consider the viscous boundary layer in the problem. Doing so, Thiévenaz et al. (2020b) considered the flow model leading to Equation 12 in the moving frame $z - h_i(t)$ and for $P \gg 1$. Using for the solid growth the Stefan model (Equation 7), $h_i(t) \sim \sqrt{D_{eff} t}$, the self-similarity analysis holds, and the scaling law is still valid with the introduction of an effective Reynolds number,

$$\beta_{max} \sim Re_{eff}^{1/5}, \qquad 13.$$

defined using the effective kinematic viscosity $\nu_{eff} = (\sqrt{\nu} + \sqrt{D_{eff}})^2$. This scaling allowed the authors to gather all their data of the impacts of water droplets in a single curve (see **Figure 5*a***). For intermediate regimes of P, the scaling also holds well for the impact of water on ice (Sarlin et al. 2024). For $P \ll 1$, this result seems not to hold anymore (Gorin et al. 2022), but one may ask whether the arrest can be due to the presence of a crystal at the contact line.

A different model can be used for the solid layer growth if the liquid is supercooled. In that case dendrites can form, and the cloud of dendrites growing from the substrate surface has a constant velocity, $h_i(t) \sim V_c\, t$. Unfortunately, in this case, the self-similarity solution is lost; Schremb et al. (2018) explored the solution numerically. Their experiments measured the residual ice layer thickness in an impact performed with supercooled water on a small post of ice (the radius grows larger than the post so only the residual solid layer can be measured). The numerical model agrees fairly well with the experimental measurements.

To summarize, the drop spreads and forms a lamella of height $h(t)$ and radius $r(t)$. At the same time, a solid layer grows vertically with a thickness $h_i(t)$ and a radius $r_i(t)$. The discussion above mentioned that the arrest happens if the viscous boundary layer reaches the free surface ($P \gg 1$), if

the capillarity prevents the spreading ($P \ll 1$), or if the contact line is caught by a growing crystal ($\dot{r} < \dot{r}_i$, which we scale as $U < V_c$). These three regimes are drawn in **Figure 5*c*** as a tentative regime map to be confirmed experimentally. The effect of the solidification should thus not be observed for low undercoolings and high Re_{eff} in the viscous arrest region.

It should be noted that an alternative could be to use microhydrodynamics models developed for wetting (Ralston et al. 2008). Shikhmurzaev (2021) extended this model and remarked that "dynamic wetting and solidification are actually particular cases in a wide class of flows where interfaces form and/or disappear" (Shikhmurzaev 2023). In this framework, numerical computation for the onset of solidification (when a liquid is put in contact with a cool solid wall) recovers the Stefan solution at long times and identifies a new behavior at early times where the solid–liquid interface temperature evolves nonmonotonously before the formation of ice (Belozerov & Shikhmurzaev 2022). These recent findings remain to be tested experimentally. Finally, one has to notice intriguing recent results for water impacting on silicon wafers where β_{max} is found to vary nonmonotonically with ΔT (Shang et al. 2020, Yang et al. 2023).

2.1.2.4. Morphology of the ice splat. Previously, we focused on the mechanisms at play that could explain why and how a droplet will stop spreading due to solidification. Once the drop stops spreading after a very short time τ_s, a second phase takes place in which the solid layer grows in the remaining liquid part. We briefly review here the recent experiments performed with water drops impacting on cold surfaces. The main structures of ice observed experimentally are presented in **Figure 6**. Once the droplet reaches its maximal extent, the contact line stays pinned at the icy edge during a certain time τ_{SCL} before receding during a time τ_{rec}. We will see in the third part of this review the complexity behind this receding behavior and the implication it has on the wetting of water on its own ice. During this whole process, the ice layer grows continuously in a typical time τ_{sol}. If $\tau_{sol} > \tau_{SCL} + \tau_{rec}$, the water film retracts to form a droplet that will ultimately freeze, as illustrated in **Figure 6*a*** (Thiévenaz et al. 2019). If $\tau_{SCL} < \tau_{sol} < \tau_{SCL} + \tau_{rec}$, the retracting film is caught while receding, leading to ring shapes that can be seen in **Figure 6*b*,*c*** (Hu et al. 2020, Thiévenaz et al. 2020a, Fang et al. 2021). Finally, if $\tau_{sol} < \tau_{SCL}$, the film does not even start to retract and a basin shape is observed as in **Figure 6*d*** (Wang et al. 2019). At even later times, upon continuous cooling, the ice will shrink, generating internal stresses that will ultimately lead to cracks as can be seen in **Figure 1** (Ghabache et al. 2016, Shen et al. 2024) or even self-peeling (Fang et al. 2022).

2.2. Water Films Freezing

Exploring the interplay between solidification and capillary flows requires going beyond the case of the droplet. Different geometries and complexities can be studied. Indeed, complex aqueous

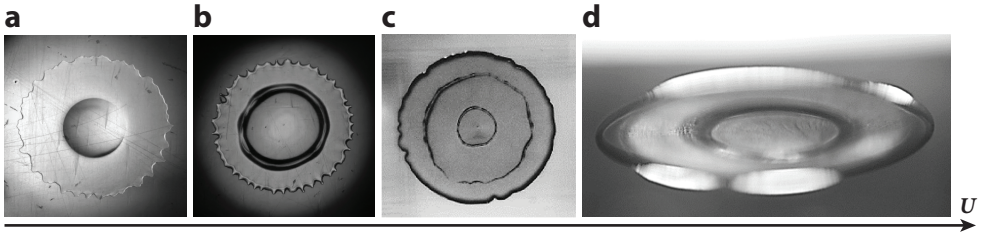

Figure 6

Final shape of the frozen water drop after impact, as the impact velocity increases: (*a*) pancake, (*b*) single ring, (*c*) double ring, and (*d*) basin geometries. The splats have a typical diameter of 1 cm. Panels *a* and *b* adapted with permission from Thiévenaz et al. (2020a). Panels *c* and *d* adapted with permission from Fang et al. (2021).

FREEZING AND SOFT MATTER

With the conviction that a physical understanding of the freezing process of soils could be of interest, researchers started to apply the knowledge of solidification of alloys to model systems for soils, which are suspensions of particles (Rempel & Worster 1999, Peppin et al. 2008, Saint-Michel et al. 2017). With a different goal, Deville et al. (2006) controlled the interactions between particles and a freezing front to build architectured materials. From these pioneering studies, the wetting condition between the ice and the particles in the suspension appeared crucial and called for precisely designed experiments. A major experimental breakthrough was made by Dedovets et al. (2018) when a setup was built where one could independently control the temperature gradient and the velocity of the freezing front. Placing this setup under a confocal microscope with different dyes allows for the clear visualization of the front at the microscopic scale. This technique was recently used to explore the interaction of a front with unique particles (solids or drops), highlighting the importance of thermal and solutal effects (Tyagi et al. 2020, 2022).

This experimental technique also allows for the precise mapping of mechanical forces developing around the solidification front (Gerber et al. 2022, 2023; Yang et al. 2024), pointing at the importance of ice crystallinity and local effects to understand the flows triggered by a solidifying front. These local effects also are of prime importance when one looks at the engulfment of a deformable object into the ice, whether a bubble (Meijer et al. 2024, Thiévenaz et al. 2024) or a drop (Meijer et al. 2023, van Buuren et al. 2024).

Finally, all these recent advances could shed new light on complex processes such as the solidification of an assembly of bubbles (a foam) (Bumma et al. 2023; K. Bumma, A. Huerre, T. Séon & J. Pierre, unpublished manuscript) and could also inspire new interactions between freezing fronts and soft materials (see **Figure 3*c***) (Séguy et al. 2024).

media such as foams or soils lead to various phenomena upon freezing (see the sidebar titled Freezing and Soft Matter). For the case of film water flows, we detail below the scarce results obtained mainly for 1D and axisymmetric geometries.

2.2.1. The rivulet, a 1D freezing flow. To further explore the coupling of a forced flow, a free surface, and a solidification front, Monier et al. (2020) studied the case of a rivulet flowing down a freezing inclined plane. With time, an ice layer grows and the rivulet shape is maintained, with water flowing on the ice structure. The ice growth at early times is well described by the Stefan equation with no influence of the flow. However, the dynamics soon deviates from the classic behavior and the ice layer thickness saturates after a few minutes in the experiments (see an example of the ice structure in **Figure 1*f***). Qualitatively, the water must cool down to the solidification temperature T_m while flowing down the icy slope. However, the cooling heat flux is inversely proportional to the ice thickness. As a result, cooling becomes less effective as the ice thickness increases. Eventually, the ice thickness becomes too great for the water to be brought to T_m before reaching the bottom of the slope, leading to a stationary state. The authors also proposed a model based on thermal exchanges and water flow to account for the results (Huerre et al. 2021). A thermal boundary layer develops in the water from the ice and reaches the free surface, decreasing the measured surface temperature. A good agreement between the theory and the measurements highlights the role of the free-surface confinement in the geometry of the ice structure built.

2.2.2. Axisymmetric flow, the icicle. Icicles are created when water flows in a cold environment and slowly solidifies on the previously created ice. During this process, solidification releases latent heat that diffuses through the flowing water film (the flow velocities are small and convection in the liquid is neglected) and is then transferred to the surrounding cold air. Earlier attempts to

model this phenomenon considered the natural boundary layer flow generated in the air by the warm body nearby (the water). This model predicted a universal conelike shape (Short et al. 2006), imperfectly representing the wide variety of shapes obtained in the extensive set of experimental data gathered by Chen & Morris (2011). Attention in the field then shifted to the explanation of the wavelength of the ripples observed at the surface of the icicles. Due to surface tension, the liquid layer flowing on the ripples has a varying thickness. Regions with smaller thicknesses transfer heat more efficiently and thus will grow more ice. On the other hand, the flow and the surface tension will oppose the development of the rippled pattern at the liquid–air interface. An instability is triggered and the typical length of the emerging pattern is found to be in good agreement with ripples measured in experiments (Ueno 2007). However, it was pointed out that in experiments, ripples do not appear for pure water icicles (Chen & Morris 2013) but some impurities, like salt, are necessary. Moreover, very recent studies (Ladan & Morris 2021, 2022; Demmenie et al. 2023) clearly showed with dyed water that the flow is not a film covering the entire icicle but a rivulet exploring different paths over time. These observations contradict the main hypothesis of the models proposed earlier (purely thermal, axisymmetric flow) and call for a deeper understanding of the flow of water on its own ice. The existence of these rivulets reveals the nonwetting tendency of the water on the ice in these conditions. The following part of this review is consequently dedicated to the question of the wetting of water on ice.

γ_{iw}, γ_{wg}, and γ_{ig}: surface tension between, respectively, the ice and the water, the water and the gas, and the ice and the gas

3. ON THE WETTING OF WATER ON ICE

As illustrated in the previous part, understanding the capillary flows of water on ice and the macroscopic structures formed by the freezing of these capillary flows requires understanding the wetting behavior of water on ice. This section gathers and presents important concepts related to this complex and still-debated subject.

3.1. Introduction to Wetting

The wetting behavior of a liquid drop on a solid substrate is driven by the competition between the cohesive forces within the liquid, which cause the drop to ball up and avoid contact with the surface, and the adhesive forces between the liquid and solid, which cause the liquid drop to spread across the surface (Bonn et al. 2009, Israelachvili 2011). In this section, we focus on the particular case where ice is the solid and water is the liquid. Therefore, three surface tensions need to be considered: ice–water, water–air, and ice–air. Young's equation gives the relation between the equilibrium contact angle θ the drop makes with the ice and the three surface tensions:

$$\gamma_{ig} = \gamma_{iw} + \gamma_{wg} \cos\theta. \qquad 14.$$

The surface tensions are, at least, defined when the three phases are in mechanical equilibrium. The system should also be at thermal equilibrium; unfortunately, in this review we sometimes have to consider an effective contact angle out of thermodynamic equilibrium.

The spreading parameter is defined as $S = \gamma_{ig} - (\gamma_{iw} + \gamma_{wg})$. When $S < 0$ a drop on ice adopts a finite contact angle; this configuration is called partial wetting. On the other hand, $S \geq 0$ implies the contact angle is zero and a water layer covers the whole solid, which is the so-called complete wetting situation. It is important to realize that in our system the surface tensions between ice and vapor γ_{ig} and ice and water γ_{iw} are not known precisely enough to allow us to determine the contact angle or the spreading parameter. We come back to this point in the last part of this section. To complete the definition of the wetting behavior, we need to consider the intermolecular interactions involved.

3.2. Van der Waals Forces Between Surfaces

Discussing the intermolecular interactions between two surfaces, we first recall the concept of disjoining pressure. We then present a more complete framework applied specifically to ice.

Hamaker constant (A): gives the amplitude of the interaction; $A \simeq 10^{-19}$ J for condensed phases whether solid or liquid bounding vacuum

Thickness (D): thickness of the water film separating the two media (ice and air); D is larger than the molecular size

3.2.1. Disjoining pressure and the Hamaker constant. We consider a liquid film of thickness D on a solid substrate (see **Figure 2*b***). The total excess surface free energy per unit area is $W_{tot}(D) = \gamma_{iw} + \gamma_{wg} + W_{vdW}(D)$, with $W_{vdW}(D)$ the van der Waals forces contribution due to the finite size of the film [$W_{vdW}(\infty) \equiv 0$]. The equilibrium wetting properties of water on ice are mainly a consequence of the net effect of the van der Waals interactions.

The van der Waals interactions ($\propto 1/r^6$) include all intermolecular dipole–dipole (Keesom forces), dipole–induced dipole (Debye forces), and induced dipole–induced dipole (London dispersion forces) interactions. By integrating this interatomic van der Waals pair potential over all atoms present in the two half-spaces bounding the film of thickness D (see **Figure 2*b***), one ends up with the interaction energy per unit surface area of two planes at a distance D apart: $W_{vdW}(D) = -\frac{A}{12\pi D^2}$.

The pressure between the two flat surfaces is derived from the van der Waals interaction energy per unit surface and is called the disjoining pressure:

$$\Pi(D) = -\frac{dW_{vdW}(D)}{dD} = -\frac{A}{6\pi D^3}. \quad 15.$$

When A is negative, the pressure is repulsive and the system can lower its free energy by increasing the distance D between the two surfaces, which leads to a wetting film. In the opposite case, A is positive, the pressure is attractive, and the water film thickness D decreases, leading to a dewetting film. Considering the spreading parameter S, the wetting will be complete if A is negative and S is positive. On the other hand, if A is positive, wetting will be incomplete, whatever the sign of S (Brochard-Wyart et al. 1991). Consequently, the Hamaker constant, and therefore more generally the van der Waals forces' contribution to the total excess surface free energy W_{vdW}, is a key property for determining the wetting behavior. Note in particular for water planar surfaces in contact ($D \simeq 0.2$ nm and $A = 1.5 \times 10^{-19}$ J), the adhesion energy is about -100 mJ m^{-2}, which corresponds to a surface energy of $\gamma = -W_{vdW}/2 = 50$ mJ m^{-2}, very close to the surface tension of water.

3.2.2. Ice interface, retardation, and incomplete melting. In the subtle experiments in which ice, at temperatures below 0°C, is observed to slowly surface melt (Bartels-Rausch et al. 2014), a particularly interesting behavior is observed but not captured in the previous nonretarded framework. This case of the surface melting of ice demands a more complete calculation of van der Waals forces, applying the general theory of Dzyaloshinskii, Lifshitz, and Pitaevskii (DLP) (Lifshitz 1956, Dzyaloshinskii et al. 1961) to ice, water, and vapor at the triple point. This was carried out by Elbaum and Schick in 1991 (Elbaum & Schick 1991, Dash et al. 2006, Israelachvili 2011).

The assumption of simple pairwise additivity neglects the influence of neighboring atoms on the interaction between any pair of atoms. In particular, the effective polarizability of each atom is influenced by the field of any other atoms around. In the DLP theory, sometimes called the macroscopic theory of van der Waals forces, the atomic structure is ignored and the van der Waals forces between the macroscopic bodies, 1 and 2, interacting across a medium, 3, now treated as continuous media, are derived in terms of bulk properties. In this framework, the dielectric properties of the three materials are characterized by their frequency-dependent polarizability, and the interaction energy $W_{vdW}(D)$ is calculated by integrating the dipolar interactions over all frequencies.

In their work, Elbaum & Schick (1991) pointed out that the polarizability of ice is greater than that of water at frequencies higher than the ultraviolet, whereas it is smaller at lower frequencies. Knowing that wetting occurs when the polarizability of a substrate is greater than that of a film, we expect that wetting of water on ice should not happen when low frequencies dominate over high frequencies. In addition, the dispersion contribution to the van der Waals forces can start suffering attenuation, due to the finite speed of light, when the distance between the molecules involved becomes greater than a few nanometers; this effect is called retardation. The zero-frequency orientation and induction energy remain nonretarded at all separations. Consequently, the authors showed that as long as the surface melted layer of water is thin, the polarizabilities at all frequencies contribute additively to the wetting forces, and the water wets the ice. However, when the water layer is thickening, retardation reduces the high-frequency contributions of dispersion forces, typically higher than the ultraviolet, and favors those in which the polarizability of ice is smaller than that of water: The wetting behavior changes from wetting to dewetting. In terms of the Hamaker constant, everything happens as if it were changing sign from negative to positive. The nonwetting behavior of water on ice is a consequence of the frequency-dependent dispersion forces of the van der Waals interactions.

Retardation: attenuation of the dispersion contribution to the van der Waals forces due to the finite speed of light

Quasi-liquid layer: premelting layer on ice surface

In this thick water layer case, typically 3 nm in the calculation of Elbaum & Schick (1991), the water film free surface is attracted by the ice and the water layer stops growing, leading to so-called incomplete melting. The additional liquid will dewet and form droplets that stand on the previously formed film. This particular state is also called pseudopartial wetting (Brochard-Wyart et al. 1991). The authors conclude that a macroscopically thick liquid film is therefore not permitted at the ice–vapor interface at the triple point.

3.3. Surface Premelting of Ice

In the system considered here, the layer between air and crystalline ice, disordered on a molecular scale, is called the ice surface premelting layer, ice premelt, or quasi-liquid layer. It forms at the ice surface for temperatures below 0°C. It plays a crucial role in the lubrication of ice (Rosenberg 2005), cloud physics (Dash et al. 2006), frost heave (Wettlaufer & Worster 2006), and regelation (freezing/melting by changing pressure) (Drake & Shreve 1973). Most likely, the first mention of a premelting layer in the literature relates precisely to regelation, stemming from Faraday's famous experiment in which two ice cubes freeze together upon contact (Faraday 1859, 1860). Since then, it has been widely studied (Fletcher 1962, Dash et al. 2006, Li & Somorjai 2007, Bartels-Rausch et al. 2014, Nagata et al. 2019, Slater & Michaelides 2019) and is still the subject of passionate debate. In particular, among the questions left unanswered are the thickness of the premelting layer, spanning from 1 to 100 nm, its variation with temperature, and its onset temperature (see Bartels-Rausch et al. 2014, figure 7). These uncertainties are mostly due to a huge sensitivity to perturbations and experimental conditions. In the following, we focus on recent experimental observations of the structure of this ice surface premelting layer.

The theoretical prediction of Elbaum & Schick (1991) introduced previously suggests that, as ice premelts, the premelted layer thickens and reaches a pseudopartial wetting situation, in which drops form on the film when the thickness exceeds a critical value. Two years later, Elbaum et al. (1993) published an experimental observation of the surface premelting of ice in pure water vapor; they showed that the melt layer increases slowly up to 20 nm as ice is warmed, after which droplets form on the wetting film without mixing, in line with their prediction, except for the wetting layer thickness.

Since that study, major experimental developments have enabled us to better understand and quantify the appearance of this particular structure over an ice surface (Nagata et al. 2019,

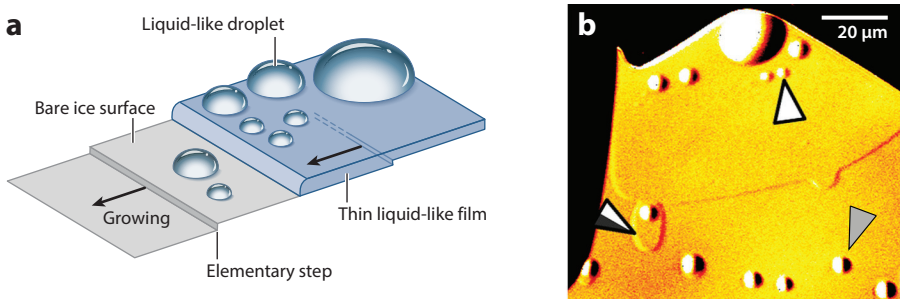

Figure 7

(*a*) Schematic illustration of the surface premelting of ice. Panel adapted with permission from Sazaki et al. (2013); copyright American Chemical Society. (*b*) The appearance of quasi-liquid droplets and a thin quasi-liquid layer on an ice basal face under relatively high supersaturation conditions. The white and black-and-white arrowheads show quasi-liquid droplets and quasi-liquid film phases, respectively. The gray arrowhead shows quasi-liquid droplets on bare ice. The quasi-liquid droplets and film are distributed inhomogeneously in space. The image was obtained using laser confocal microscopy combined with differential interference contrast microscopy (Sazaki et al. 2004), which can directly visualize the 0.37-nm-thick elementary steps on ice crystal surfaces (Sazaki et al. 2010, 2014). Panel adapted with permission from Asakawa et al. (2016) and Slater & Michaelides (2019).

Slater & Michaelides 2019). Premelting of the ice crystal surface starts from the disordering of the topmost layer at the ice–air interface (Murata et al. 2016, Pickering et al. 2018). This disordering is due to the rupture of hydrogen bonds of the water molecules in the topmost layer. The onset temperature at which disordering of the topmost layer first appears is still debated (Qiu & Molinero 2018), but recent results place it at ∼−90°C (Nagata et al. 2019) or −70°C (Wei et al. 2001, 2002; Shultz 2017). Then, as the temperature rises, the hydrogen bond breakdown spreads to the next few layers, also making them disordered. When the temperature reaches ∼−2°C, quasi-liquid droplets and a film start to emerge. Gen Sazaki and coworkers (Sazaki et al. 2012, Asakawa et al. 2016, Murata et al. 2016) made a breakthrough in the fine visualization of the ice premelting surface in the range −2.15 to −0.25°C. Their crucial finding was the observation of micrometric water droplets on bare ice and on quasi-liquid film, respectively in partial wetting and pseudopartial wetting conditions, as shown in **Figure 7**. They observed that the droplets can coalesce and form a film coating the crystal. The quasi-liquid film has been determined to be 9 ± 3 nm thick (Furukawa et al. 1987, Murata et al. 2015) at −1.75°C. A pressure–temperature diagram for quasi-liquid droplets and films is provided by Murata et al. (2016) and Nagata et al. (2019). The coexistence of quasi-liquid droplets and films suggests that these phases are distinct.

Among these three distinct types of quasi-liquid states—disordered layers, quasi-liquid droplets, and quasi-liquid films—the first is formed under equilibrium conditions and the latter two under nonequilibrium conditions. Also, it is interesting to note that quasi-liquid droplets and films can be formed by surface condensation associated with supersaturation or by surface melting associated with undersaturation (Murata et al. 2016). Finally, all this experimental work highlights the dynamic and nearly bidimensional multiphase complex structure of the premelting ice surface, mainly composed of nonwetting droplets and wetting films.

3.4. Nature of the Topmost Disordered Layer

We saw that above the onset temperature, the topmost layer at the ice–air interface becomes disordered because it experiences the first ruptures of hydrogen bonds. This enables the interfacial

water molecules to exchange a hydrogen bond and, consequently, to increase their mobility (Weber et al. 2018). The following is dedicated to briefly discussing the nature of this disordered layer and the mechanism of the water molecules' mobility. A key question that leads to some controversy is whether the surface can be described with a liquid phase analogy or not. It is an important question to improve our understanding of the surface chemistry of ice under freezing conditions, in particular because of its influence on the wetting behavior.

A theoretical study (Henson et al. 2005) in agreement with experimental results (Döppenschmidt & Butt 2000) indicated that the quasi-liquid layer is simply equivalent to ordinary deeply supercooled water. On the other hand, simulations and experimental observations suggest that the disordered layer is more similar to ice than to supercooled liquid water (Bartels-Rausch et al. 2014). In particular, Sánchez et al. (2017) confirmed this idea, showing that the quasi-liquid layer has stronger hydrogen bonds than liquid water. Other experiments, using either interfacial force microscopy (Goertz et al. 2009) or nanorheology (Canale et al. 2019), suggested that the quasi-liquid layer is neither ice nor water (Shultz 2017) as it exhibits complex viscoelastic properties, with a viscosity up to two orders of magnitude greater than that of pure water. Alternatively, the numerical study of Pickering et al. (2018) affirms, in accordance with an older study (Hudait et al. 2017), that the topmost disordered layers are largely nonhomogeneous spatially, composed of islands of solid water a few nanometers in length surrounded by liquid regions. They found this structure with a typical content of 40% liquid as low as −23°C, well below the first appearance of quasi-liquid droplets (Sazaki et al. 2012).

To gain insight into the nature of this disordered layer, the mobility of water molecules at the ice surface, which is much less understood than in bulk ice (Petrenko & Whitworth 1999), should be examined. It is well accepted that, within the quasi-liquid layer, properties are different than in the bulk; in particular, water molecule transport is much faster (Bartels-Rausch et al. 2014). Typically, the surface diffusion coefficient has been determined, by measuring the time formation of a groove on a heated polycrystal (Mullins 1957), to be five orders of magnitude larger than the self-diffusion coefficient in crystalline bulk ice at the same temperature. Interestingly, it is very close to the value of supercooled water (Nasello et al. 2007). But despite these close values of the diffusion coefficient, an Arrhenius analysis of the self-diffusion coefficient shows opposite variations of energy of activation with temperature on the ice surface and in bulk supercooled water (Gladich et al. 2011). This implies that water molecules' mobility is caused by significantly different mechanisms in each system. More recently, an experiment of spontaneous scratch healing on ice, with temperatures ranging from −30 to −0.5°C (Demmenie et al. 2022) (see **Figure 8**), proposed that the dominant water molecule mobility mechanism is local sublimation from the ice surface followed by condensation onto the ice surface, instead of surface diffusion or local evaporation from a quasi-liquid layer. Indeed, it is noteworthy that ice has a vapor pressure much

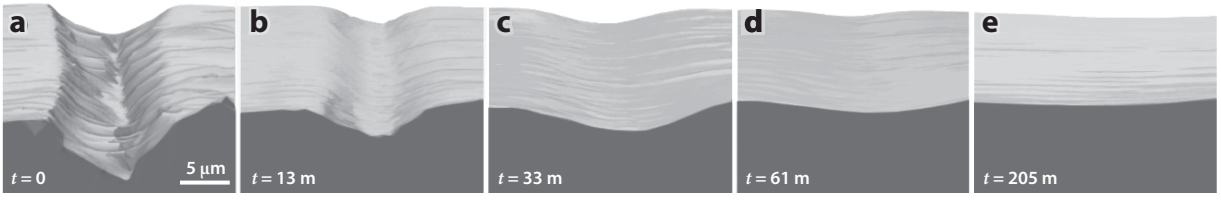

Figure 8

Evolution of a scratch in ice (initial depth ∼2.5 μm) healing in time under controlled conditions, with a constant ice temperature of 247 K and vapor pressure at equilibrium. The high vapor pressure of ice explains the relatively quick healing process. Figure adapted from Demmenie et al. (2022) (CC BY 4.0).

higher than almost all other solids. This study points toward a description of the ice surface as a solid rather than a liquid.

Finally, the nature of the disordered quasi-liquid premelted layer is still the subject of intense debate, and more effort will be needed to improve the description of this complex phase, which still appears to be a hybrid between solid and liquid.

3.5. The Water–Ice–Air Contact Angle

As we saw before, there now seems to be a consensus on the fact that water should not completely wet the ice. We conclude this section with a presentation of the existing measurements of the contact angle of water on ice. Note that the contact angle measurement may be uncertain due to imperfect equilibrium, inadequate proof of purity, and the often unknown ice–water interface shape at the contact angle.

Starting at the quasi-liquid film and droplet scale, Elbaum & Schick (1991) estimated the contact angle of the predicted nano-quasi-liquid droplet in a pseudopartial wetting condition to be 0.2°. In a companion paper, Elbaum et al. (1993) experimentally observed droplets on top of an 18-nm quasi-liquid layer under vapor and measured a contact angle of 0.6°. More recently, when the pseudopartial and partial wetting conditions coexist (as in **Figure 7**) Murata et al. (2016) measured a wetting angle of the quasi-liquid droplet (∼10 μm) on both a quasi-liquid film and bare ice surface to be small and very similar: 0.6° and 0.8°, respectively. When quasi-liquid droplets are only in a partial wetting state, the same authors measured their contact angle on bare ice to be 2.3°. This suggests that changing the wettability of the quasi-liquid system, by changing the vapor pressure or the temperature, results in a change of the premelted layer microstructure. Note that, at a similar scale, Ketcham & Hobbs (1969) deduced the contact angle of a water film on ice by measuring its thickness and found it to be 1°.

Considering Young's relation (Equation 14) and knowing the surface tension of water at 0°C, $\gamma_w = 75.6$ mJ m^{-2} (Lide 2005), the contact angle of water on ice could be deduced from the knowledge of the surface free energy of ice γ_{ig} and the interfacial tension between ice and water γ_{iw}. Unfortunately, today these values are not known precisely enough to discriminate between 0 and ∼50°. Indeed, the ice–water interfacial free energy γ_{iw} is found to be in the range of 27 to 35 mJ m^{-2} (Espinosa et al. 2016, Ambler et al. 2017) and the surface tension of ice γ_{ig} in the range of 70 to 120 mJ m^{-2} at 0°C (de Reuck 1957, Ketcham & Hobbs 1969, Van Oss et al. 1992, Djikaev & Ruckenstein 2017).

Consequently, in order to know the macroscopic wetting condition of water on ice, the contact angle has been measured in various situations. One of the first measurements was realized by Knight (1966). He deposited a puddle of liquid water on a cold copper substrate and measured a contact angle of 12° at a temperature slightly below 0°C. Depending on whether a contact angle hysteresis exists or not (de Gennes et al. 2013), this angle may be an equilibrium or a receding angle. A few years later he realized other measurements in various configurations (Knight 1971) and found different values. Finally, he concluded in 1996 (Knight 1996) that measuring this angle unequivocally may be impossible but indications are that it is not zero. Makkonen (1997) proposed that the static equilibrium contact angle of a water drop at a temperature close to 95°C deposited on ice at −25°C is around 37°. Recently, Demmenie et al. (2023) conducted experiments with sessile water droplets on ice and concluded that the contact angle varies with the ice temperature from 40° at −10°C up to 12° close to the melting temperature.

In Thiévenaz and colleagues' (2020a) experiment with drop impact on a cold surface described at the end of Section 2.1.2, we saw that, after a given time, a film of water retracts on a growing ice layer and forms either a drop or a ring (**Figure 6*a*,*b***). In the first case, when the retracting water

Table 2 Experimental values of the ice–water–air contact angle

Method	Contact angle values
Microscale measurements	0.2–2.3°
Young's relation	0–50°
Macroscopic drop measurements[a]	12–40°
Dynamic wetting	6–12°

[a]The values found depend on the substrate temperature.

film has time to build an equilibrium spherical cap before being frozen, the authors show that its contact angle with the ice always reaches a constant limit value of ∼12°, for any control parameters. This angle is an equilibrium or a receding angle, but in either case, it exists and is unique and constant. Finally, recently Grivet et al. (2024) carried out a Landau–Levich-type experiment in which an ice sheet is pulled out of a water bath. At low speeds, there is a range of parameters in which the water film is not entrained, and its height along the ice allowed the authors to deduce a receding contact angle between water and ice. This original measurement of the contact angle of water on ice predicts a value of 6° with an accuracy of a few degrees.

In conclusion, the existence of a nonzero contact angle between water and ice is well accepted nowadays. However, its measurement still spans quite a large range, from 0.6° up to 40° (see **Table 2**). It seems that the contact angle at the microscale is always significantly smaller than the one measured in macroscopic experiments. In the temperature range where the quasi-liquid film and droplets exist, they might form a precursor film upstream of the macroscopic contact line. The small angle would be the one of the precursor film with ice, and the one measured at a macroscopic scale an apparent contact angle of a contact line in a pseudopartial wetting condition. The value of the contact angle, static or dynamic, made by a drop or a film of water on ice is crucial to improving our understanding of the formation of ice structures by water flow or impact. It is also of prime importance for the design of icephobic surfaces (Kreder et al. 2016), and there is still a lot of work to be done to achieve this goal.

FUTURE ISSUES

1. The dendritic theoretical description needs to be generalized in order to encompass the propagation of a crystal in a cold liquid in contact with a cold solid.
2. The arrest of the contact line by a crystal raises the question of the force of the pinning, linking the problem to the wetting.
3. Propagation of the solidification front in complex systems such as hydrogel or unsaturated granular material still needs to be investigated, along with the modification of these complex structures after a cycle of solidification and melting.
4. The complex ice structure formed by the continuous flow of a water film in a cold environment encompasses most of the scientific questions addressed in this review, and, even more, remains a completely open question.
5. Original numerical methods still need to be developed to account for all solid–ice–liquid–air phases. In particular, a method able to deal with the moving contact lines in air–liquid–ice and air–liquid–solid systems is still lacking. Hybrid approaches are key to such further development.

6. The question of the value of the equilibrium contact angle of water on ice, and its potential hysteresis, at 0°C is still open. Its definition out of thermal equilibrium needs to be clarified and subsequently its dependence with the temperature should be studied in more detail.

DISCLOSURE STATEMENT

The authors are not aware of any affiliations, memberships, funding, or financial holdings that might be perceived as affecting the objectivity of this review.

ACKNOWLEDGMENTS

We warmly thank the Cargèse Institute for Science for hosting the InterFreeze summer school and all the speakers there for inspiring presentations and discussions. We also thank the members of the Frozen Team for all the discussions in recent years: Virgile Thiévenaz, Antoine Monier, Simon Brient, Rodolphe Grivet, Pierre-Antoine Maës, Krishan Bumma, Lila Séguy, Hélie de Miramon, Alexandre Limare, Mathilde Tavares, Wladimir Sarlin, Juliette Pierre, Suzie Protière, Laurent Duchemin, and Stéphane Popinet. A.H. is supported by the Mairie de Paris Emergences Program and C.J. by Agence de l'Innovation de Défense via Centre Interdisciplinaire d'Etudes pour la Défense et la Sécurité (project 2021 - ICING).

LITERATURE CITED

Ambler M, Vorselaars B, Allen MP, Quigley D. 2017. Solid–liquid interfacial free energy of ice Ih, ice Ic, and ice 0 within a mono-atomic model of water via the capillary wave method. *J. Chem. Phys.* 146(7):074701

Anderson D, Worster MG, Davis S. 1996. The case for a dynamic contact angle in containerless solidification. *J. Cryst. Growth* 163(3):329–38

Anderson DM, Guba P. 2020. Convective phenomena in mushy layers. *Annu. Rev. Fluid Mech.* 52:93–119

Asakawa H, Sazaki G, Nagashima K, Nakatsubo S, Furukawa Y. 2016. Two types of quasi-liquid layers on ice crystals are formed kinetically. *PNAS* 113(7):1749–53

Attinger D, Zhao Z, Poulikakos D. 2000. An experimental study of molten microdroplet surface deposition and solidification: transient behavior and wetting angle dynamics. *J. Heat Transf.* 122(3):544–56

Aziz SD, Chandra S. 2000. Impact, recoil and splashing of molten metal droplets. *Int. J. Heat Mass Transf.* 43(16):2841–57

Bartels-Rausch T, Jacobi HW, Kahan TF, Thomas JL, Thomson ES, et al. 2014. A review of air–ice chemical and physical interactions (AICI): liquids, quasi-liquids, and solids in snow. *Atmos. Chem. Phys.* 14(3):1587–633

Belozerov AA, Shikhmurzaev YD. 2022. The onset of solidification: from interface formation to the Stefan regime. *J. Chem. Phys.* 156(19):194701

Bhola R, Chandra S. 1999. Parameters controlling solidification of molten wax droplets falling on a solid surface. *J. Mater. Sci.* 34:4883–94

Biance AL, Clanet C, Quéré D. 2004. First steps in the spreading of a liquid droplet. *Phys. Rev. E* 69(1):016301

Boettinger WJ, Warren JA, Beckermann C, Karma A. 2002. Phase-field simulation of solidification. *Annu. Rev. Mater. Res.* 32:163–94

Bonn D, Eggers J, Indekeu J, Meunier J, Rolley E. 2009. Wetting and spreading. *Rev. Mod. Phys.* 81(2):739–805

Boulogne F, Salonen A. 2020. Drop freezing: fine detection of contaminants by measuring the tip angle. *Appl. Phys. Lett.* 116(10):103701

Brochard-Wyart F, Di Meglio JM, Quére D, De Gennes PG. 1991. Spreading of nonvolatile liquids in a continuum picture. *Langmuir* 7(2):335–38

Bumma K, Huerre A, Pierre J, Séon T. 2023. Early freezing dynamics of an aqueous foam. *Soft Matter* 19:5379–84
Canale L, Comtet J, Niguès A, Cohen C, Clanet C, et al. 2019. Nanorheology of interfacial water during ice gliding. *Phys. Rev. X* 9(4):041025
Chang S, Song H, Wu K. 2021. Experimental investigation on impact dynamics and freezing performance of water droplet on horizontal cold surface. *Sustain. Energy Technol. Assess.* 45:101128
Chen ASH, Morris SW. 2011. Experiments on the morphology of icicles. *Phys. Rev. E* 83(2):026307
Chen ASH, Morris SW. 2013. On the origin and evolution of icicle ripples. *New J. Phys.* 15(10):103012
Dash J, Rempel A, Wettlaufer J. 2006. The physics of premelted ice and its geophysical consequences. *Rev. Mod. Phys.* 78(3):695
de Gennes P-G, Brochard-Wyart F, Quéré D. 2013. *Capillarity and Wetting Phenomena: Drops, Bubbles, Pearls, Waves*. New York: Springer
de Reuck A. 1957. The surface free energy of ice. *Nature* 179(4570):1119–20
de Ruiter J, Soto D, Varanasi KK. 2018. Self-peeling of impacting droplets. *Nat. Phys.* 14(1):35–39
de Ruiter R, Colinet P, Brunet P, Snoeijer JH, Gelderblom H. 2017. Contact line arrest in solidifying spreading drops. *Phys. Rev. Fluids* 2(4):043602
Dedovets D, Monteux C, Deville S. 2018. Five-dimensional imaging of freezing emulsions with solute effects. *Science* 360(6386):303–6
Demmenie M, Kolpakov P, Nagata Y, Woutersen S, Bonn D. 2022. Scratch-healing behavior of ice by local sublimation and condensation. *J. Phys. Chem. C* 126(4):2179–83
Demmenie M, Reus L, Kolpakov P, Woutersen S, Bonn D, Shahidzadeh N. 2023. Growth and form of rippled icicles. *Phys. Rev. Appl.* 19(2):024005
Deville S, Saiz E, Nalla RK, Tomsia AP. 2006. Freezing as a path to build complex composites. *Science* 311(5760):515–18
Djikaev Y, Ruckenstein E. 2017. Self-consistent determination of the ice–air interfacial tension and ice–water–air line tension from experiments on the freezing of water droplets. *J. Phys. Chem. C* 121(30):16432–39
Döppenschmidt A, Butt HJ. 2000. Measuring the thickness of the liquid-like layer on ice surfaces with atomic force microscopy. *Langmuir* 16(16):6709–14
Drake L, Shreve R. 1973. Pressure melting and regelation of ice by round wires. *Proc. R. Soc. A* 332(1588):51–83
Dzyaloshinskii IE, Lifshitz EM, Pitaevskii LP. 1961. The general theory of van der Waals forces. *Adv. Phys.* 10(38):165–209
Elbaum M, Lipson S, Dash J. 1993. Optical study of surface melting on ice. *J. Cryst. Growth* 129(3–4):491–505
Elbaum M, Schick M. 1991. Application of the theory of dispersion forces to the surface melting of ice. *Phys. Rev. Lett.* 66(13):1713–16
Espinosa JR, Vega C, Sanz E. 2016. Ice–water interfacial free energy for the TIP4P, TIP4P/2005, TIP4P/ice, and mW models as obtained from the mold integration technique. *J. Phys. Chem. C* 120(15):8068–75
Fanfoni M, Tomellini M. 1998. The Johnson-Mehl-Avrami-Kolmogorov model: a brief review. *Nuovo Cimento D* 20(7–8):1171–82
Fang W-Z, Zhu F, Tao W-Q, Yang C. 2021. How different freezing morphologies of impacting droplets form. *J. Colloid Interface Sci.* 584:403–10
Fang W-Z, Zhu F, Zhu L, Tao W-Q, Yang C. 2022. Self-peeling of frozen water droplets upon impacting a cold surface. *Commun. Phys.* 5(1):51
Faraday M. 1859. *Experimental Researches in Chemistry and Physics*. London: Taylor & Francis
Faraday M. 1860. I. Note on regelation. *Proc. R. Soc. Lond.* 10:440–50
Favier B, Purseed J, Duchemin L. 2019. Rayleigh–Bénard convection with a melting boundary. *J. Fluid Mech.* 858:437–73
Feltham DL, Untersteiner N, Wettlaufer JS, Worster MG. 2006. Sea ice is a mushy layer. *Geophys. Res. Lett.* 33(14):L14501
Fletcher NH. 1962. Surface structure of water and ice. *Philos. Mag.* 7(74):255–69
Furukawa Y, Yamamoto M, Kuroda T. 1987. Ellipsometric study of the transition layer on the surface of an ice crystal. *J. Cryst. Growth* 82(4):665–77
Gent RW, Dart NP, Cansdale JT. 2000. Aircraft icing. *Philos. Trans. R. Soc. A* 358(1776):2873–911

Gerber D, Wilen LA, Dufresne ER, Style RW. 2023. Polycrystallinity enhances stress build-up around ice. *Phys. Rev. Lett.* 131(20):208201
Gerber D, Wilen LA, Poydenot F, Dufresne ER, Style RW. 2022. Stress accumulation by confined ice in a temperature gradient. *PNAS* 119(31):e2200748119
Ghabache E, Josserand C, Séon T. 2016. Frozen impacted drop: from fragmentation to hierarchical crack patterns. *Phys. Rev. Lett.* 117(7):074501
Gibou F, Fedkiw R, Osher S. 2018. A review of level-set methods and some recent applications. *J. Comput. Phys.* 353:82–109
Gielen MV, de Ruiter R, Koldeweij RBJ, Lohse D, Snoeijer JH, Gelderblom H. 2020. Solidification of liquid metal drops during impact. *J. Fluid Mech.* 883:A32
Gladich I, Pfalzgraff W, Maršálek O, Jungwirth P, Roeselová M, Neshyba S. 2011. Arrhenius analysis of anisotropic surface self-diffusion on the prismatic facet of ice. *Phys. Chem. Chem. Phys.* 13(44):19960–69
Goertz M, Zhu XY, Houston J. 2009. Exploring the liquid-like layer on the ice surface. *Langmuir* 25(12):6905–8
Gorin B, Bonn D, Kellay H. 2022. Droplet impacts on cold surfaces. *J. Fluid Mech.* 944:A23
Grivet R, Huerre A, Séon T, Duchemin L, Josserand C. 2024. Freezing receding contact lines. arXiv:2409.00385 [physics.flu-dyn]
Grivet R, Huerre A, Séon T, Josserand C. 2023. Making superhydrophobic splashes by surface cooling. *Phys. Rev. Fluids* 8(6):063603
Grivet R, Monier A, Huerre A, Josserand C, Séon T. 2022. Contact line catch up by growing ice crystals. *Phys. Rev. Lett.* 128(25):254501
Henson B, Voss L, Wilson KR, Robinson J. 2005. Thermodynamic model of quasiliquid formation on H_2O ice: comparison with experiment. *J. Chem. Phys.* 123(14):144707
Herbaut R, Brunet P, Limat L, Royon L. 2019. Liquid spreading on cold surfaces: solidification-induced stick-slip dynamics. *Phys. Rev. Fluids* 4(3):033603
Herbaut R, Dervaux J, Brunet P, Royon L, Limat L. 2020. A criterion for the pinning and depinning of an advancing contact line on a cold substrate. *Eur. Phys. J. Spec. Top.* 229(10):1867–80
Hu M, Wang F, Tao Q, Chen L, Rubinstein SM, Deng D. 2020. Frozen patterns of impacted droplets: from conical tips to toroidal shapes. *Phys. Rev. Fluids* 5(8):081601
Hudait A, Allen MT, Molinero V. 2017. Sink or swim: ions and organics at the ice–air interface. *J. Am. Chem. Soc.* 139(29):10095–103
Huerre A, Monier A, Séon T, Josserand C. 2021. Solidification of a rivulet: shape and temperature fields. *J. Fluid Mech.* 914:A32
Israelachvili JN. 2011. *Intermolecular and Surface Forces*. Amsterdam: Elsevier. 3rd ed.
Jaafar MA, Rousse DR, Gibout S, Bédécarrats JP. 2017. A review of dendritic growth during solidification: mathematical modeling and numerical simulations. *Renew. Sustain. Energy Rev.* 74:1064–79
Josserand C, Thoroddsen ST. 2016. Drop impact on a solid surface. *Annu. Rev. Fluid Mech.* 48:365–91
Jung S, Tiwari MK, Doan NV, Poulikakos D. 2012a. Mechanism of supercooled droplet freezing on surfaces. *Nat. Commun.* 3(1):615
Jung S, Tiwari MK, Poulikakos D. 2012b. Frost halos from supercooled water droplets. *PNAS* 109(40):16073–78
Juric D, Tryggvason G. 1996. A front-tracking method for dendritic solidification. *J. Comput. Phys.* 123(1):127–48
Kant P, Koldeweij RBJ, Harth K, van Limbeek MAJ, Lohse D. 2020. Fast-freezing kinetics inside a droplet impacting on a cold surface. *PNAS* 117(6):2788–94
Ketcham W, Hobbs P. 1969. An experimental determination of the surface energies of ice. *Philos. Mag.* 19(162):1161–73
Khain AP, Pinsky M. 2018. Microphysical processes in ice and mixed-phase clouds. In *Physical Processes in Clouds and Cloud Modeling*, pp. 344–496. Cambridge, UK: Cambridge Univ. Press
Knight CA. 1966. The contact angle of water on ice. *J. Colloid Interface Sci.* 25(2):280–84
Knight CA. 1971. Experiments on the contact angle of water on ice. *Philos. Mag.* 23(181):153–65
Knight CA. 1996. Surface layers on ice. *J. Geophys. Res. Atmos.* 101(D8):12921–28

Koldeweij RBJ, Kant P, Harth K, de Ruiter R, Gelderblom H, et al. 2021. Initial solidification dynamics of spreading droplets. *Phys. Rev. Fluids* 6(12):L121601
Kreder MJ, Alvarenga J, Kim P, Aizenberg J. 2016. Design of anti-icing surfaces: smooth, textured or slippery? *Nat. Rev. Mater.* 1(1):15003
Laan N, de Bruin KG, Bartolo D, Josserand C, Bonn D. 2014. Maximum diameter of impacting liquid droplets. *Phys. Rev. Appl.* 2(4):044018
Ladan J, Morris SW. 2021. Experiments on the dynamic wetting of growing icicles. *New J. Phys.* 23(12):123017
Ladan J, Morris SW. 2022. Pattern of inclusions inside rippled icicles. *Phys. Rev. E* 106(5):054211
Lamé G, Clapeyron B. 1831. Mémoire sur la solidification par refroidissement d'un globe liquide. *Ann. Chim. Phys.* 47:250–56
Langer JS. 1980. Instabilities and pattern formation in crystal growth. *Rev. Mod. Phys.* 52(1):1–28
Lewandowski JJ, Seifi M. 2016. Metal additive manufacturing: a review of mechanical properties. *Annu. Rev. Mater. Res.* 46:151–86
Li R, Ashgriz N, Chandra S, Andrews J, Drappel S. 2008. Deposition of molten ink droplets on a solid surface. *J. Imaging Sci. Technol.* 52(2):20502-1–20502-10
Li Y, Somorjai GA. 2007. Surface premelting of ice. *J. Phys. Chem. C* 111(27):9631–37
Lide DR. 2005. *CRC Handbook of Chemistry and Physics*. Boca Raton, FL: CRC Press
Lifshitz EM. 1956. The theory of molecular attractive forces between solids. *Sov. Phys. JETP* 2(1):73–83
Limare A, Popinet S, Josserand C, Xue Z, Ghigo A. 2023. A hybrid level-set / embedded boundary method applied to solidification-melt problems. *J. Comput. Phys.* 474:111829
Lolla VY, Ahmadi SF, Park H, Fugaro AP, Boreyko JB. 2022. Arrested dynamics of droplet spreading on ice. *Phys. Rev. Lett.* 129(7):074502
Loulou T, Delaunay D. 1997. The interface temperature of two suddenly contacting bodies, one of them undergoing phase change. *Int. J. Heat Mass Transf.* 40(7):1713–16
Lyu S, Wang K, Zhang Z, Pedrono A, Sun C, Legendre D. 2021. A hybrid VOF-IBM method for the simulation of freezing liquid films and freezing drops. *J. Comput. Phys.* 432:110160
Madejski J. 1976. Solidification of droplets on a cold surface. *Int. J. Heat Mass Transf.* 19(9):1009–13
Makkonen L. 1997. Surface melting of ice. *J. Phys. Chem. B* 101(32):6196–200
Marín A, Enríquez O, Brunet P, Colinet P, Snoeijer J. 2014. Universality of tip singularity formation in freezing water drops. *Phys. Rev. Lett.* 113(5):054301
McGuire AD, Lawrence DM, Koven C, Clein JS, Burke E, et al. 2018. Dependence of the evolution of carbon dynamics in the northern permafrost region on the trajectory of climate change. *PNAS* 115(15):3882–87
Meijer JG, Bertin V, Lohse D. 2023. Frozen Cheerios effect: particle-particle interaction induced by an advancing solidification front. arXiv:2311.09477 [cond-mat.soft]
Meijer JG, Rocha D, Linnenbank AM, Diddens C, Lohse D. 2024. Enhanced bubble growth near an advancing solidification front. arXiv:2402.06409 [physics.flu-dyn]
Miao S, Zhang C, Liu X. 2024. Tunable tip singularity of a water droplet freezing on surfaces under forced convection. *Appl. Therm. Eng.* 241:122362
Monier A, Huerre A, Josserand C, Séon T. 2020. Freezing a rivulet. *Phys. Rev. Fluids* 5(6):062301
Moore MR, Mughal MS, Papageorgiou DT. 2017. Ice formation within a thin film flowing over a flat plate. *J. Fluid Mech.* 817:455–89
Mullins WW. 1957. Theory of thermal grooving. *J. Appl. Phys.* 28(3):333–39
Mullins WW, Sekerka RF. 1964. Stability of a planar interface during solidification of a dilute binary alloy. *J. Appl. Phys.* 35(2):444–51
Murata K-i, Asakawa H, Nagashima K, Furukawa Y, Sazaki G. 2015. In situ determination of surface tension-to-shear viscosity ratio for quasiliquid layers on ice crystal surfaces. *Phys. Rev. Lett.* 115(25):256103
Murata K-i, Asakawa H, Nagashima K, Furukawa Y, Sazaki G. 2016. Thermodynamic origin of surface melting on ice crystals. *PNAS* 113(44):E6741–48
Nagata Y, Hama T, Backus EHG, Mezger M, Bonn D, et al. 2019. The surface of ice under equilibrium and nonequilibrium conditions. *Acc. Chem. Res.* 52(4):1006–15
Nasello OB, de Juarez SN, Di Prinzio CL. 2007. Measurement of self-diffusion on ice surface. *Scr. Mater.* 56(12):1071–73

Nauenberg M. 2013. Comment on "Pointy ice-drops: How water freezes into a singular shape" [Am. J. Phys. 80, 764–771 (2012)]. *Am. J. Phys.* 81(2):150–51
Nauenberg M. 2016. Theory and experiments on the ice–water front propagation in droplets freezing on a subzero surface. *Eur. J. Phys.* 37(4):045102
Neufeld JA, Goldstein RE, Worster MG. 2010. On the mechanisms of icicle evolution. *J. Fluid Mech.* 647:287–308
Pasandideh-Fard M, Bhola R, Chandra S, Mostaghimi J. 1998. Deposition of tin droplets on a steel plate: simulations and experiments. *Int. J. Heat Mass Transf.* 41(19):2929–45
Peppin SSL, Wettlaufer JS, Worster MG. 2008. Experimental verification of morphological instability in freezing aqueous colloidal suspensions. *Phys. Rev. Lett.* 100(23):238301
Petrenko VF, Whitworth RW. 1999. *Physics of Ice*. Oxford, UK: Clarendon Press
Pickering I, Paleico M, Sirkin YAP, Scherlis DA, Factorovich MH. 2018. Grand canonical investigation of the quasi liquid layer of ice: Is it liquid? *J. Phys. Chem. B* 122(18):4880–90
Plapp M. 2011. Remarks on some open problems in phase-field modelling of solidification. *Philos. Mag.* 91(1):25–44
Poulikakos D, Attinger D, Zhao Z. 2002. Heat transfer and solidification during the impact of a droplet on a surface. In *Drop-Surface Interactions*, ed. M Rein, pp. 159–84. CISM Int. Cent. Mech. Sci. Courses Lect. Vol. 456. Vienna: Springer
Qiu Y, Molinero V. 2018. Why is it so difficult to identify the onset of ice premelting? *J. Phys. Chem. Lett.* 9(17):5179–82
Ralston J, Popescu M, Sedev R. 2008. Dynamics of wetting from an experimental point of view. *Annu. Rev. Mater. Res.* 38:23–43
Rempel AW, Worster MG. 1999. The interaction between a particle and an advancing solidification front. *J. Cryst. Growth* 205(3):427–40
Reuther K, Rettenmayr M. 2014. Simulating dendritic solidification using an anisotropy-free meshless front-tracking method. *J. Comput. Phys.* 279:63–66
Roisman IV. 2010a. Fast forced liquid film spreading on a substrate: flow, heat transfer and phase transition. *J. Fluid Mech.* 656:189–204
Roisman IV. 2010b. On the instability of a free viscous rim. *J. Fluid Mech.* 661:206–28
Roisman IV, Tropea C. 2021. Wetting and icing of surfaces. *Curr. Opin. Colloid Interface Sci.* 53:101400
Rosenberg R. 2005. Why is ice slippery? *Phys. Today* 58(12):50–54
Saint-Michel B, Georgelin M, Deville S, Pocheau A. 2017. Interaction of multiple particles with a solidification front: from compacted particle layer to particle trapping. *Langmuir* 33(23):5617–27
Sánchez MA, Kling T, Ishiyama T, van Zadel MJ, Bisson PJ, et al. 2017. Experimental and theoretical evidence for bilayer-by-bilayer surface melting of crystalline ice. *PNAS* 114(2):227–32
Sarlin W, Grivet R, Xu J, Huerre A, Séon T, Josserand C. 2024. Role of melting and solidification in the spreading of an impacting water drop. *J. Fluid Mech.* 996:A14
Sazaki G, Asakawa H, Nagashima K, Nakatsubo S, Furukawa Y. 2013. How do quasi-liquid layers emerge from ice crystal surfaces? *Cryst. Growth Des.* 13(4):1761–66
Sazaki G, Asakawa H, Nagashima K, Nakatsubo S, Furukawa Y. 2014. Double spiral steps on I_h ice crystal surfaces grown from water vapor just below the melting point. *Cryst. Growth Des.* 14(5):2133–37
Sazaki G, Matsui T, Tsukamoto K, Usami N, Ujihara T, et al. 2004. In situ observation of elementary growth steps on the surface of protein crystals by laser confocal microscopy. *J. Cryst. Growth* 262(1–4):536–42
Sazaki G, Zepeda S, Nakatsubo S, Yokomine M, Furukawa Y. 2012. Quasi-liquid layers on ice crystal surfaces are made up of two different phases. *PNAS* 109(4):1052–55
Sazaki G, Zepeda S, Nakatsubo S, Yokoyama E, Furukawa Y. 2010. Elementary steps at the surface of ice crystals visualized by advanced optical microscopy. *PNAS* 107(46):19702–7
Schetnikov A, Matiunin V, Chernov V. 2015. Conical shape of frozen water droplets. *Am. J. Phys.* 83(1):36–38
Schiaffino S, Sonin AA. 1997a. Motion and arrest of a molten contact line on a cold surface: an experimental study. *Phys. Fluids* 9(8):2217–26
Schiaffino S, Sonin AA. 1997b. On the theory for the arrest of an advancing molten contact line on a cold solid of the same material. *Phys. Fluids* 9(8):2227–33

Schremb M, Roisman IV, Tropea C. 2017. Transient effects in ice nucleation of a water drop impacting onto a cold substrate. *Phys. Rev. E* 95(2):022805

Schremb M, Roisman IV, Tropea C. 2018. Normal impact of supercooled water drops onto a smooth ice surface: experiments and modelling. *J. Fluid Mech.* 835:1087–107

Schultz WW, Worster MG, Anderson DM. 2001. Solidifying sessile water droplets. In *Interactive Dynamics of Convection and Solidification*, ed. P Ehrhard, DS Riley, PH Steen, pp. 209–26. Dordrecht, Neth.: Springer

Sebilleau J, Ablonet E, Tordjeman P, Legendre D. 2021. Air humidity effects on water-drop icing. *Phys. Rev. E* 104(3):L032802

Séguy L, Protière S, Huerre A. 2023. Role of geometry and adhesion in droplet freezing dynamics. *Phys. Rev. Fluids* 8(3):033601

Séguy L, Huerre A, Protière S. 2024. Deformation of hydrogel during freezing. arXiv:2410.06766 [cond-mat.soft]

Shang Y, Zhang Y, Hou Y, Bai B, Zhong X. 2020. Effects of surface subcooling on the spreading dynamics of an impact water droplet. *Phys. Fluids* 32(12):123309

Shen F, Fang WZ, Zhu FQ, Chai D, Tao WQ. 2024. Freezing behaviors of an impacting droplet on subcooled hydrophobic surfaces. *Appl. Therm. Eng.* 236:121535

Shibkov A, Zheltov M, Korolev A, Kazakov A, Leonov A. 2005. Crossover from diffusion-limited to kinetics-limited growth of ice crystals. *J. Cryst. Growth* 285(1–2):215–27

Shikhmurzaev YD. 2021. Solidification and dynamic wetting: a unified modeling framework. *Phys. Fluids* 33(7):072101

Shikhmurzaev YD. 2023. *Interaction of non-isothermal flow and solidification*. Presented at the 4th International Conference on Fluid Flow and Thermal Science, Lisbon

Short MB, Baygents JC, Goldstein RE. 2006. A free-boundary theory for the shape of the ideal dripping icicle. *Phys. Fluids* 18(8):083101

Shultz MJ. 2017. Ice surfaces. *Annu. Rev. Phys. Chem.* 68:285–304

Slater B, Michaelides A. 2019. Surface premelting of water ice. *Nat. Rev. Chem.* 3(3):172–88

Stairs RA. 1971. Changes of drop-shapes on freezing. *Anal. Chem.* 43(11):1535–36

Stiti M, Castanet G, Labergue A, Lemoine F. 2020. Icing of a droplet deposited onto a subcooled surface. *Int. J. Heat Mass Transf.* 159:120116

Taber S. 1930. The mechanics of frost heaving. *J. Geol.* 38(4):303–17

Tavakoli F, Davis SH, Kavehpour HP. 2014. Spreading and arrest of a molten liquid on cold substrates. *Langmuir* 30(34):10151–55

Tavares M, Josserand C, Limare A, Lopez-Herrera J-M, Popinet S. 2024. A coupled VOF/embedded boundary method to model two-phase flows on arbitrary solid surfaces. *Comput. Fluids* 278:106317

Thiévenaz V, Josserand C, Séon T. 2020a. Retraction and freezing of a water film on ice. *Phys. Rev. Fluids* 5(4):041601

Thiévenaz V, Meijer JG, Lohse D, Sauret A. 2024. Universal equation describes the shape of air bubbles trapped in ice. arXiv:2402.13456 [cond-mat.soft]

Thiévenaz V, Séon T, Josserand C. 2019. Solidification dynamics of an impacted drop. *J. Fluid Mech.* 874:756–73

Thiévenaz V, Séon T, Josserand C. 2020b. Freezing-damped impact of a water drop. *Europhys. Lett.* 132(2):24002

Tryggvason G, Scardovelli R, Zaleski S. 2011. *Direct Numerical Simulations of Gas–Liquid Multiphase Flows*. Cambridge, UK: Cambridge Univ. Press. 1st ed.

Tyagi S, Huynh H, Monteux C, Deville S. 2020. Objects interacting with solidification fronts: thermal and solute effects. *Materialia* 12:100802

Tyagi S, Monteux C, Deville S. 2022. Solute effects on the dynamics and deformation of emulsion droplets during freezing. *Soft Matter* 18:4178–88

Ueno K. 2007. Characteristics of the wavelength of ripples on icicles. *Phys. Fluids* 19(9):093602

Ulvrová M, Labrosse S, Coltice N, Råback P, Tackley P. 2012. Numerical modelling of convection interacting with a melting and solidification front: application to the thermal evolution of the basal magma ocean. *Phys. Earth Planet. Inter.* 206:51–66

van Buuren D, Kant P, Meijer JG, Diddens C, Lohse D. 2024. Deforming ice with drops. arXiv:2402.18947 [physics.flu-dyn]

Van Oss CJ, Giese RF, Wentzek R, Norris J, Chuvilin EM. 1992. Surface tension parameters of ice obtained from contact angle data and from positive and negative particle adhesion to advancing freezing fronts. *J. Adhes. Sci. Technol.* 6(4):503–16

Walford MER, Hargreaves DM, Stuart-Smith S, Lowson M. 1991. Freezing of water drops on a cold surface. *J. Glaciol.* 37(125):47–50

Wang L, Kong W, Wang F, Liu H. 2019. Effect of nucleation time on freezing morphology and type of a water droplet impacting onto cold substrate. *Int. J. Heat Mass Transf.* 130:831–42

Weady S, Tong J, Zidovska A, Ristroph L. 2022. Anomalous convective flows carve pinnacles and scallops in melting ice. *Phys. Rev. Lett.* 128(4):044502

Weber B, Nagata Y, Ketzetzi S, Tang F, Smit WJ, et al. 2018. Molecular insight into the slipperiness of ice. *J. Phys. Chem. Lett.* 9(11):2838–42

Wei X, Miranda PB, Shen Y. 2001. Surface vibrational spectroscopic study of surface melting of ice. *Phys. Rev. Lett.* 86(8):1554–57

Wei X, Miranda PB, Zhang C, Shen Y. 2002. Sum-frequency spectroscopic studies of ice interfaces. *Phys. Rev. B* 66(8):085401

Wettlaufer JS, Worster MG. 2006. Premelting dynamics. *Annu. Rev. Fluid Mech.* 38:427–52

Worster MG. 2000. Solidification of fluids. In *Perspectives in Fluid Dynamics: A Collective Introduction to Current Research*, ed. GK Batchelor, HK Moffatt, MG Worster, pp. 393–446. Cambridge, UK: Cambridge Univ. Press

Yang S, Gerber D, Feng Y, Bain N, Kuster M, et al. 2024. Dehydration drives damage in the freezing of brittle hydrogels. *Sci. Adv.* 10(34):eado7750

Yang S, Zhang Z, Liu X, Lai T, Hou Y. 2023. Spreading dynamics of a droplet impacts on a supercooled substrate: physical models and neural networks. *Colloids Surf. A Physicochem. Eng. Aspects* 677:132381

Yarin A. 2006. Drop impact dynamics: splashing, spreading, receding, bouncing.... *Annu. Rev. Fluid Mech.* 38:159–92